RSC Advances

PAPER

View Article Online
View Journal | View Issue

Cite this: *RSC Adv.*, 2025, **15**, 24202

Mechanistic investigation of mild steel corrosion inhibition by *Codiaeum variegatum* extract: weight loss, EIS, and DFT perspectives†

Aashu Singh Solanki,[a] Ankit Sharma,[a] Shobhana Sharma,[*b] Abhinay Thakur*[c] and Sushil Kumar Sharma[*a]

The corrosion inhibition efficacy of *Codiaeum variegatum* leaf extract (CVLE) on mild steel in 1 N HCl was assessed utilizing weight-loss (WL), potentiodynamic polarization (PDP), and electrochemical impedance spectroscopy (EIS) methods at different temperatures 298 K, 308 K, 318 K, 328 K and 338 K. The study revealed that CVLE is an environmentally friendly and sustainable corrosion inhibitor, attaining an impressive inhibition efficacy of 91.83 ± 0.04% at 1000 ppm concentration at 298 K. A significant reduction in corrosion rate (C_R) from 21.264 ± 0.02 to 1.735 ± 0.05 mmpy and corrosion current density (i_{corr}) from 157.63 ± 0.01 to 4.02 ± 0.02 μA cm^{-2} was observed with increasing CVLE concentration, highlighting its protective efficacy. The adsorption of CVLE followed the Langmuir adsorption isotherm on the mild steel surface, indicating monolayer adsorption behavior. Potentiodynamic polarization studies classified CVLE as a mixed-type inhibitor, influencing both cathodic and anodic reactions. The mechanism of inhibition occurring on mild steel was discovered using the XPS method. Scanning electron microscopy (SEM) confirmed the creation of a layer of protection by CVLE on the mild steel surface, corroborating its inhibitory action. EIS analysis further demonstrated that the inhibiting efficacy was elevated with higher concentrations of CVLE, consistent with a rise in adsorption equilibrium constant (K_{ads}), indicating stronger inhibitor–metal interactions. Theoretical studies supported these findings by showing a low energy gap (ΔE), signifying strong adsorption and excellent anti-corrosion potential of CVLE at the molecular level. This inclusive study establishes CVLE as an effective and eco-friendly inhibitor for mild steel corrosion in acidic environments.

Received 3rd May 2025
Accepted 3rd July 2025

DOI: 10.1039/d5ra03125g

rsc.li/rsc-advances

1. Introduction

A ubiquitous and natural process, corrosion results in substantial financial losses, pollution of the environment, metal deterioration, and possible risks to human health and the ecosystem.[1] Because of its superior mechanical and physical qualities, mild steel is used in a variety of engineering, building, military, and equipment applications. The fact that mild steel corrodes severely in acidic, and aggressive conditions including pickling, descaling, and acidizing oil well media is a serious worry.[2] Acidic solutions based on HCl are used in several industries for chemical cleaning and pickling. Mild steel corrodes quickly as a result, which has several negative effects, such as a decrease in mechanical and physical strength, structural deterioration or breakdown, and fluid intrusion in pipelines and containers, which lead drop in product pricing.[3] As a result, current research focuses on determining how to regulate the rate of corrosion. The usage of corrosion inhibitors is the most successful option for mitigating corrosion among the several approaches. Organometallic complexes,[4–7] organic inhibitors,[8] and ionic liquids[9,10] have all been employed as corrosion inhibitors to reduce mild steel corrosion thus far. It is well known that organic molecules can adsorb onto metal surfaces through chemical or physical interactions, especially those containing polar functional groups or heteroatoms.[11–13] Because this adsorption blocks electrochemical processes on the metal surface at both cathodic and anodic locations, it creates protective barrier-type coatings that stop corrosion.[14–16] Unfortunately, a lot of commercial corrosion inhibitors are expensive, and some of them might be dangerous to human health and the surroundings.[17,18] Concerns about human health and environmental degradation are becoming more and more important to governments and researchers worldwide, as are important for growing economies and cultures.[10] As a result,

[a]*Department of Pure and Applied Chemistry, University of Kota, Kota, Rajasthan, 324005, India. E-mail: sushil@uok.ac.in; shobhna.sharma51@gmail.com; thakurabhinay96@gmail.com*

[b]*Department of Chemistry, S. S. Jain Subodh P G College, Jaipur, Rajasthan, 302004, India*

[c]*Division of Research and Development, Lovely Professional University, Phagwara, Punjab, 144411, India*

† Electronic supplementary information (ESI) available: Fig. S1–S3 pertaining to immersion are accessible in the supporting documentation. See DOI: https://doi.org/10.1039/d5ra03125g

developing effective corrosion inhibitors, reasonably priced, and environmentally friendly has taken precedence.[19] Green corrosion inhibitors are becoming more and more well-liked as environmentally acceptable and sustainable substitutes for traditional and hazardous corrosion inhibitors. They are produced using natural resources like biomass, weevils, shrubs, and plants. Extracts from these natural sources have several benefits, including low environmental impact, non-toxicity, competitive price, efficiency, and accessibility.[20,21] Among the phytochemicals present in these extracts are phenolic compounds, alkaline, tannins, catechin, terpenoids, flavonoids, and saponin.[20,21] Because of their many bonds and electron-rich polar functional components, these compounds can adhere to substrates of metal rapidly and create a protective layer that inhibits too many corrosion ions from penetrating, thus hindering metallic corrosion. Compared to conventional inhibitors, these eco-friendly inhibitors are less harmful to the surroundings and biodegradable. They are also a prospective substitute for commercial and industrial applications due to their diversity and ease of large-scale acquisition.[22–24] Recent research has demonstrated how well natural sources work as corrosion inhibitors to stop metallic corrosion. Thakur *et al.*,[25] for instance, examined the effectiveness of *Cnicus Benedictus* aerial extract in halting the corrosion of mild steel in 0.5 M HCl. According to electrochemical tests, *Cnicus Benedictus* extract, which relates to the Asteraceae family, exhibits a 92.45% inhibitory efficacy at 1000 ppm and functions as a sustainable and environmentally friendly mild steel corrosion inhibitor in 0.5 M HCl media. The corrosion rate dropped dramatically from 7.4114 to 0.97438 mmpy due to the elevated levels of CBE, demonstrating the protective effect of CBE on metal. The contact angle measurements showed that a highly protective layer had been deposited on the surface of mild steel. The main goal of Mamudu *et al.*[26] was to investigate a novel method for applying *Dillenia suffruticosa* leaf extract (DSLE) on the metal in hydrochloric acid media to prevent corrosion. Using ethanol and a soxhlet system, the phytocompounds that inhibit rusting were recovered. The morphological analysis of the corroded metallic specimens with gravimetric and electrochemical techniques was used to assess the extract's efficacy as a corrosion inhibitor. Fourier-transformed infrared spectroscopy and scanning electron microscopy were used in this investigation to look at the specimens both with and without the extract added as an inhibitor. The results show that DSLE works very well to prevent mild steel from corroding in an acidic environment.

Thakur *et al.*[27] discussed the mechanistic understanding of how eco-friendly *Asphodelus Tenuifolius* (ATAE) aerial extract inhibits metallic corrosion in acidic environments. By comparing the anodic (β_a) and cathodic (β_c) polarization slope values, the electrochemical study results showed a concentration-dependent improvement in corrosion resistance, identifying ATAE as a mixed-type inhibitor. At 250 ppm, the inhibition efficiency peaked, and at 298 K, it achieved an astounding 94.40%. Higher corrosion inhibition potential was indicated by the electrochemical study, which showed a considerable rise in polarization resistance (R_p) and charge transfer resistance (R_{ct}) values together with a drop in constant phase element value to 162.94 μF. Furthermore, theoretical studies highlighted a robust interaction between the mild steel surface and ATAE, with a narrow energy gap (ΔE), suggesting superior micro-level anti-corrosion capabilities. Tan *et al.*[28] thoroughly examined the inhibitory efficacy of discarded *Arachis hypogaea* L. leaf extract in the Cu/H_2SO_4 system using both theoretical and experimental calculation techniques. The results show that the extract included four active ingredients: 2-hydroxybenzoic acid, 3-(4-hydroxy-3-methoxyphenyl)-2-propenoic acid, phthalic acid dibutyl ester, and 4-hydroxy-3-methoxycinnamic acid 3,4-dihydroxybenzoic acid which have low energy gap values, this extract effectively inhibits corrosion. Previous research has demonstrated that metallic corrosion can be successfully reduced by natural sources like plants, shrubs, bark, and herbs. By examining the efficacy of natural extract as a corrosion inhibitor, the authors of this study want to contribute to the development of affordable, environmentally friendly corrosion inhibitors that do not harm earth, aquatic or terrestrial life. This study's goal is to ascertain whether *Codiaeum Variegatum* leaf extract is an effective corrosion inhibitor. The flowering plant genus *Codiaeum*, which belongs to the *Euphorbiaceous* family, includes the species *Codiaeum Variegatum*. It is indigenous to the tropical rainforests of the Philippines, Papua New Guinea, and Australia, as well as the Moluccan islands of Indonesia.[29] Because the plant is poisonous, neither people nor pets should consume it. It is a monoecious, evergreen tropical shrub with thick, alternately orientated leaves that can reach a height of three meters. In tropical climates, crotons are valued for their striking foliage and form beautiful hedges and potted patio specimens. In traditional medicine, it is frequently used to treat a variety of conditions, such as intestinal worms, psoriasis, diarrhea, stomachaches, ulcers, and skin infections. Numerous bioactive substances, including coumarins, saponins, anthraquinones, and cardenolides, are found in the plant. Major constituents present in *Codiaeum Variegatum* leaf extract are glaucine, oxoglaucine and ellagic acid. The selection of *Codiaeum variegatum* as a corrosion inhibitor, despite its toxic nature and limited native distribution, is strategically justified. This plant is widely used in ornamental horticulture across tropical and subtropical regions, offering an abundant and underutilized source of phytochemicals. Its major constituents – glaucine, oxoglaucine, and ellagic acid – are known to possess aromatic and heteroatomic functional groups that favor strong adsorption on metal surfaces, essential for effective corrosion inhibition.[29] Furthermore, its toxicity precludes its use in food or medical contexts, making it a sustainable candidate for industrial applications where ecological degradation and human exposure are tightly controlled. Prior studies have indicated that several non-edible and even toxic plant species can serve as potent corrosion inhibitors due to their chemical structure and surface reactivity.[30,31]

Although numerous studies have explored plant extracts as green corrosion inhibitors, limited attention has been given to the use of *Codiaeum variegatum* leaf extract (CVLE), particularly in the context of a comprehensive mechanistic evaluation that combines experimental gravimetric methods, electrochemical analysis (EIS, PDP), surface characterization (SEM, EDS, XPS, FTIR), and quantum chemical modeling *via* DFT. To the best of our knowledge, this is the first integrated report that not only investigates the anticorrosive potential of CVLE in 1 N HCl but

also elucidates its mechanistic action at both macroscopic and molecular levels. This dual approach bridges the gap between empirical inhibition data and theoretical insights into adsorption behavior, offering a holistic understanding of CVLE's performance as a green inhibitor. Additionally, because of its low harmful effects, biodegradable affordability, accessibility, and environmental friendliness, CVLE represents an environmentally friendly substitute for conventional chemical inhibitors. Its application could offer a greener alternative to dangerous chemical inhibitors for preventing corrosion.

2. Materials and methods

2.1 Preparation of materials

According to Fe-SEM with EDS, the mild steel (MS) specimen used in this study has the following composition (in percentage): Zn (0.37%), Cu (0.35%), C (3.78%), O (0.50%), and the residual Fe. MS coupons were utilized in electrochemical research and weight loss methods after being manually sliced to $3.0 \times 2.0 \times 0.10$ cm^3. The various emery paper grades (60, 80, 100, 120, 220, 320, 400, 600, 800, 1000, and 1200) were used to abrade these coupons. The coupons were washed with double-distilled water, cleaned with acetone, and dried out in a moisture-free desiccator before being added to the test solution for further investigation. Double-distilled water in 36% hydrochloric acid was used to create the stock solution of hydrochloric acid (1 N) (Fisher Scientific Ltd). The working electrode for electrochemical experiments was prepared using the same composition metal.

2.2 Test solutions

The extract was tested for its inhibitory impact in a 1 N HCl medium, which is one of the most common harsh corrosion agents. Several CVLE concentrations (200, 400, 600, 800, and 1000 ppm) were mixed with HCl, and the ideal dosage was chosen. A suitable concentration of CVLE was incorporated into a 1 N HCl solution to create a standard stock solution with 1000 ppm extract. By diluting the stock media with the appropriate HCl solution, additional required concentrations were achieved. Newly developed test solutions were used for each exam. Throughout the procedures, the solutions were not mixed and were instead left in the air. The experiments were conducted at a temperature of 298 K, 308 K, 318 K, 328 K and 338 K.

2.3 Preparation of CVLE

The leaves of *Codiaeum Variegatum* were gathered from the Kota city neighborhood and washed with double-distilled water. After being chopped into tiny pieces and allowed to dry in the shade for approximately 30 days, the leaves were ground into a powder using a grinder mixer. For 48 hours, 50 grams of the material were extracted using pure C_2H_5OH. The extract was then filtered and heated to 343 K using a Rota vapor instrument until the majority of the ethanol was evaporated. Dark black was the hue of the CVLE residue that was utilized as an inhibitor (Fig. 1). After dissolving the inhibitor in 1 N HCl, the solution was diluted to the appropriate concentration. All measurements were conducted using an inhibitor test solution, beginning with 200, 400, 600, 800, and 1000 ppm.

2.4 Weight loss method

For the weight loss investigation, MS coupons measuring $3.0 \times 2.0 \times 0.10$ cm^3 that had previously been washed and degreased were used. Previously weighed MS coupons were individually submerged for three hours at a temperature between 298–338 K in 100 mL of beaker media containing and excluding the

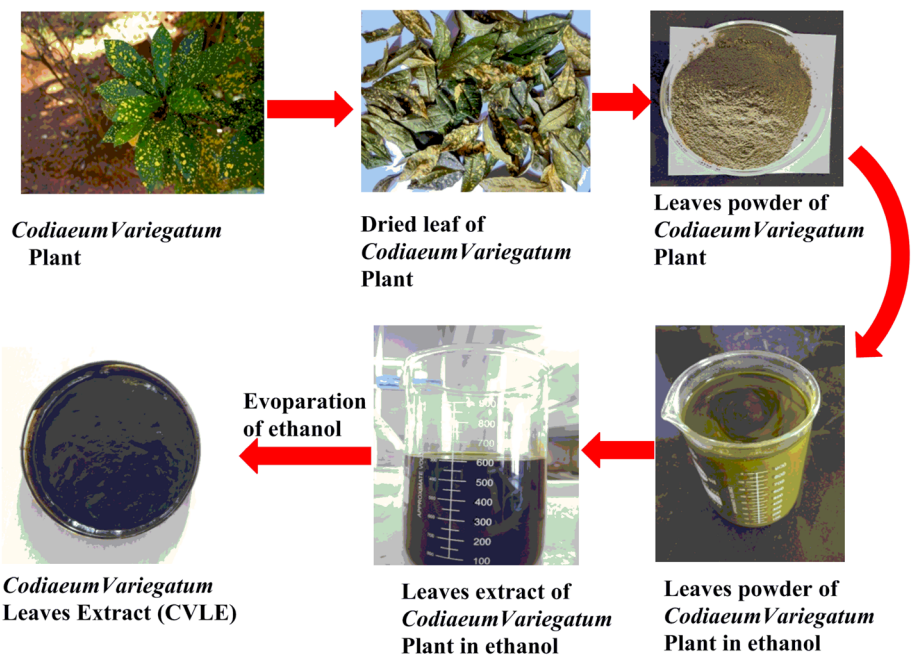

Fig. 1 Schematic representation of preparation of Leaves extract of *Codiaeum Variegatum* (CVLE).

inhibitor at several quantities, such as 200, 400, 600, 800, and 1000 ppm. After being submerged, the sample was removed and scrubbed with scouring powder free of bleach, rinsed well with water and acetone, and allowed to air dry. After that, the specimen was examined once more to determine the inhibition efficiency (IE%) and corrosion rate (C_R). While the IE% is the corrosion-inhibiting effectiveness of the inhibitor used (in a precise amount and time) to lessen the degradation of a metal or its alloys, the C_R is how quickly any metal or its alloy deteriorates in a particular environment over a given period. A freshly prepared solution was used in each assay, and its temperature was thermostatically controlled at 298 K, 308 K, 318 K, 328 K and 338 K. Eqn (1) and (2) were used to determine weight loss (ΔW) and C_R, respectively.[32]

$$\Delta W = W_0 - W_i \quad (1)$$

$$C_R = \frac{87.6\Delta W}{AtD} \quad (2)$$

A is the sample's surface area in cm^2, t is the dipping period in hours, D is the density of mild steel (7.85 g cm^{-3}), ΔW is the sample weight loss in milligrams, C_R is the corrosion rate in mmpy, and W_0 and W_i is the weight of the MS coupon before and after immersion. CVLE's corrosion inhibition effectiveness was determined using eqn (3) and (4).[33]

$$\%IE = \frac{C_{R0} - C_{Ri}}{C_{R0}} \times 100 \quad (3)$$

where C_{R0} and C_{Ri} are corrosion rates without and with inhibitor.

$$\%IE = \frac{W_0 - W_i}{W_0} \times 100 \quad (4)$$

W_0 and W_i are weight losses without and with CVLE. Surface coverage (θ) was determined using eqn (5)

$$\theta = \frac{\%IE}{100} \quad (5)$$

2.5 Electrochemical experiments

Electrochemical investigations were performed in a Potentiostat/Galvanostat Autolab-204 Metrohm, Netherlands, using a conventional three-electrode cell. Ag/AgCl in 3 M KCl as the reference electrode, graphite rod served as the counter electrode and the 1 cm^2 uncovered surface area of mild steel coupons that had been scraped, cleaned, dried, and degreased were used as working electrodes (WE).[34] The MS specimen (WE) was submerged in the test media for 30 minutes in order to achieve a reasonably steady open circuit potential (OCP) value at room temperature prior to electrochemical boundary calculations. Tafel graphs were performed at a scan rate of 0.01 V s^{-1} with a potential range of −800 mV–200 mV *vs.* OCP. The corrosion current densities were computed by examining the corrosion potential from the straight Tafel regions of the cathodic and anodic slopes. The polarization values for the Tafel curves were calculated using the software Nova version 1.10. The EIS data were recorded between 100 kHz and 0.1 Hz, with an amplitude value of ±10 mV. The Nyquist plots were recreated and the curve fitting was finished using Zsim software.

2.6 Surface morphology analysis

To assess the metallic specimens' morphology and the degree to which the CVLE molecules created a protective layer over the metallic substrate, they were immersed in a corrosive mixture (1 N HCl) for three hours at 298 K with and without CVLE (1000 ppm). The samples were taken out and dried after being submerged for three hours. Materials' ability to suppress corrosion is studied using scanning electron microscopy (SEM). SEM is an imaging method based on electrons that produces fine-grained pictures of a material's shape and surface structure. It is employed to illustrate how corrosion and the presence of inhibitors alter the surface's topography and roughness. A micro-analytical method is used in corrosion inhibition investigations to ascertain a material's elemental makeup *via* EDS. It frequently provides ESI† on the subject under study when combined with other methods, like SEM. A FEI Nova Nano FE-SEM 450 (Sydney) was utilized in this experiment, with a magnification of 50k and an accelerating voltage of 15 kV. To determine whether a protective coating had developed, the morphological properties of the corroded and uncorroded metallic substrates were analyzed. An X-ray photoelectron (XPS) analysis performed on a steel surface treated with 1000 ppm CVLE at 298 K following a 24 hour immersion in 1 N HCl verified the corrosion–prevention benefits of CVLE. ESCA+(omicron nanotechnology, Oxford Instrument, Germany) was used to take XPS reading while irradiating Al Kα source (1486.7 eV) with pass energy of 15 mA at 15 kV.

2.7 FTIR assessment

The many bioactive phytoconstituents of CVLE were identified using FTIR spectroscopy, which was also used to detect the bonding patterns and functional groups present on the metallic surface. Between 400 and 4000 cm^{-1} wavenumber, the metal surface's infrared spectrum was measured using a Tensor-27 FTIR Spectrometer with KBr pellets.

2.8 Computational analysis

Quantum chemical investigations based on Density Functional Theory (DFT) have become a widely adopted approach for studying the fundamental interactions between corrosion inhibitors and metal surfaces. Traditional methods for analyzing metal corrosion and inhibitor efficiency are often limited by factors such as time, cost, environmental concerns, and lack of precision, leading to a significant rise in the application of computational techniques like DFT.[35] This method enables a detailed evaluation of an inhibitor's effectiveness in mitigating corrosion by analyzing its chemical reactivity. In the present study, we utilized the DFT analysis using the Generalized Gradient Approximation (GGA) with the B3LYP/6-311G (++, d,p) for improved accuracy in performing theoretical calculations (16–18). The energy of the lowest unoccupied molecular

orbital (E_{LUMO}) and the highest occupied molecular orbital (E_{HOMO}) were among the characteristics that were computed, offering details into the adsorption behavior and corrosion inhibition potential of the studied inhibitor. Computational work was conducted utilizing the Gaussian 09 W software, and various quantum chemical variables were determined through eqn (6)–(12) to evaluate the inhibitor's overall reactivity and adsorption efficiency.[36]

$$\Delta E = E_{HOMO} - E_{LUMO} \quad (6)$$

$$\chi = \frac{I + A}{2} \quad (7)$$

$$\eta = \frac{I - A}{2} \quad (8)$$

$$\sigma = 1/\eta \quad (9)$$

$$\Delta N = \frac{\phi_{Fe(110)} - \chi_{inh}}{2\left(\eta_{Fe(110)} + \eta_{inh}\right)} \quad (10)$$

$$IP = -E_{HOMO} \quad (11)$$

$$EA = -E_{LUMO} \quad (12)$$

3. Result and discussion

3.1 Wight loss (WL) assessment

3.1.1 Effect of concentration. The weight loss method was used to examine the effects of different CVLE concentrations on the suppression of mild steel corrosion in 1 N HCl because of its ease of use, excellent dependability, and outstanding consistency.[37] One kind of gravimetric approach for the inhibitors' anti-corrosion action is the weight loss technique. Eqn (1)–(5) were used to evaluate the inhibitor's surface coverage, corrosion rate (C_R), and inhibition efficiency (IE) based on data from gravimetric studies.[32,33] Fig. 2 and 3 show the C_R and IE% of mild steel subjected to 1 N HCl with and without different concentrations of CVLE. According to these figures, IE% in 1 N HCl in mild steel is increased and its corrosion rate is decreased by CVLE.[38] According to Table 1, the percentage of IE increased steadily as the concentration of CVLE increased, peaking at 91.83 ± 0.04% at the highest concentration of 1000 ppm at 298 K. The results reveal that the adsorption increases along with the inhibitor's concentration, resulting in increased surface coverage. This behavior demonstrates that the inhibitor adsorption coating does, in fact, separate the mild steel surface from the destructive media.[39]

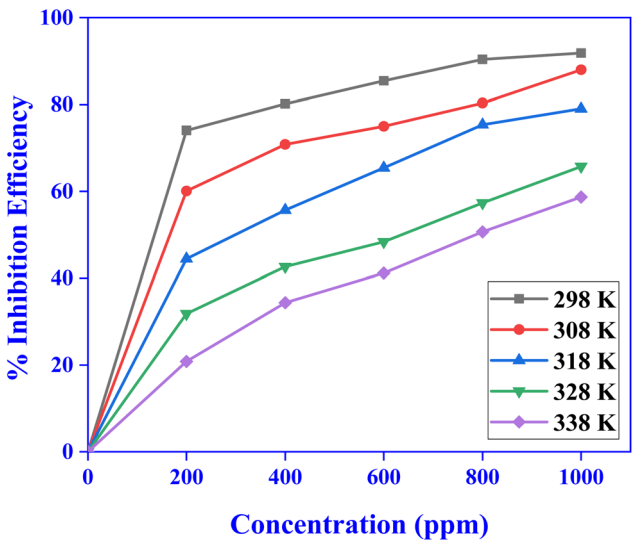

Fig. 2 %inhibition efficiency with different concentration of CVLE at various temperatures.

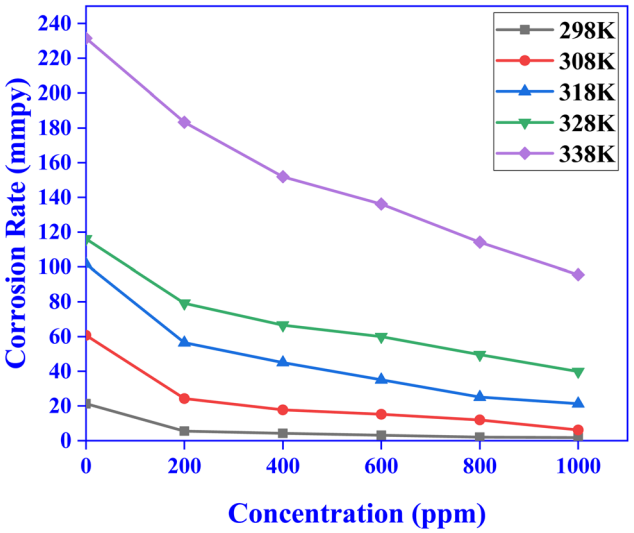

Fig. 3 C_R variation with different concentration of CVLE at various temperatures.

3.1.2 Temperature effect. An investigation report demonstrates that, due to the maximum corrosion rate at higher temperatures (Table 2), the inhibitory efficacy of CVLE gradually decreases as the temperature rises (Fig. 4). Nevertheless, even at higher temperatures, the rate of adsorption rises with increasing CVLE concentration. Because of the balance between the desorption and adsorption progressions occurring coincidentally over the mild steel coupon surface, efficiency decreases as temperature rises.[40]

3.1.3 Impact of immersion time. Table 3 illustrates how weight loss varies over time for mild steel corrosion in the absence of 1 N HCl and in the presence of 1000 ppm of CVLE over 12, 24, and 36 hours at 298 K. Immersion time is a crucial parameter which demonstrates that mild steel's weight decrease constantly rises as the amount of time without CVLE (blank coupons) grows. Without any turbidity, the light yellowish brown color of the immersion media is visible in Fig. S1–S3† display the sample conditions prior to and following the immersion period, respectively. When CVLE is present, the inhibition efficiency rises from 12 to 24 hours, and after 24 hours, the inhibition efficiency progressively falls with immersion time. At the optimal concentration (1000 ppm), the inhibition efficacy in this experiment was 87.4549 ± 0.01% for 24

Table 1 Impact of corrosion rate and inhibition effectiveness on mild steel with and without CVLE at varying concentrations

Conc. (ppm)	Inhibition efficiency (%IE)	Surface coverage (θ)	Corrosion rate (C_R) (mmpy)
Blank	—	—	21.264 ± 0.02
200	74.05 ± 0.5	0.7405 ± 0.5	5.5176 ± 0.04
400	80.17 ± 0.1	0.8017 ± 0.1	4.251 ± 0.4
600	85.42 ± 0.2	0.8542 ± 0.2	3.099 ± 0.8
800	90.37 ± 0.5	0.9037 ± 0.5	2.042 ± 0.06
1000	91.83 ± 0.04	0.9183 ± 0.04	1.735 ± 0.05

hours. The progressive decline in inhibition efficiency after 24 hours of immersion can be attributed to the gradual desorption or degradation of the protective inhibitor film over prolonged exposure. As the immersion time increases, the inhibitor molecules may lose their adherence to the mild steel surface due to sustained acidic attack, thermal agitation, or competitive adsorption by aggressive chloride ions (Cl^-) present in the 1 N HCl medium. This leads to partial exposure of the metal surface to the corrosive environment, thus reducing the overall inhibition efficiency.[41] Additionally, possible chemical transformations or breakdown of phytochemical constituents in CVLE over time could further contribute to the decreased protective ability.

The analysis was carried out at 1.0 N HCl solution, which corresponds to very low pH *i.e.* zero on Sorenson scale. Undoubtedly the pH showed be on higher level when the analysis is to be carryout out in presence of corrosion inhibitors. But as the inhibitor is of mixed type being a plant extract having polyphenolic and heteronuclear complex molecules. The polyphenolic moieties will slightly rise the $[H^+]$ concentration in the reaction medium thereby decreasing pH. On contrary the protonation of heteroatom that may be due to H^+ of acidic medium or H^+ released from the polyohenolic group of plant extract making the cathodic inhibition at the metal/solution interface. These two processes may make the concentration of H^+ in the solution at the steady state, thereby making no significant change in the pH remains zero experiments.

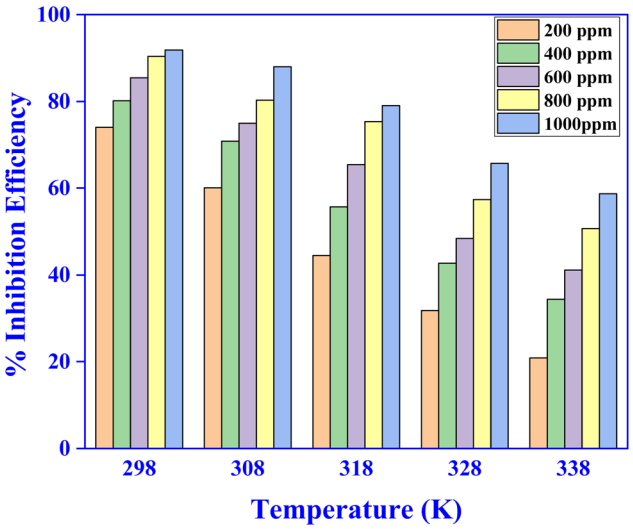

Fig. 4 Variation of % inhibition efficiency with different temperatures.

3.2 Kinetic and thermodynamic parameters

Eqn (13) and (14) of the transition state and Arrhenius theory aid in evaluating the deterioration of metal in a 1 N HCl medium and CVLE.[42] Several characteristics were calculated and entered in Table 4, including activation energy (E_a), activation enthalpy (H_a), and activation entropy (S_a).

$$\ln C_R = \ln A - E_a/RT \quad (13)$$

$$C_R = RT/Nh\exp(\Delta S_a/R)\exp - (\Delta H_a/RT) \quad (14)$$

here, C_R, E_a, h, N, T, R, A, ΔS_a, and ΔH_a stand for corrosion rate, activation energy, Planck's and Avogadro's constant, temperature, universal gas constant, pre-exponential factor, entropy of activation, and enthalpy of activation, respectively.

Table 2 Changes in mild steel corrosion rate and inhibition effectiveness with and without CVLE at different temperatures over a three-hour immersion period

Conc. (ppm)	IE (%)					C_R (mmpy)				
	298 K	308 K	318 K	328 K	338 K	298 K	308 K	318 K	328 K	338 K
Blank	—	—	—	—	—	21.264 ± 0.02	60.693 ± 0.6	101.673 ± 0.03	116.118 ± 0.04	231.492 ± 0.04
200	74.05 ± 0.5	60.07 ± 0.04	44.45 ± 0.5	31.82 ± 0.03	20.83 ± 0.1	5.5176 ± 0.04	24.240 ± 0.8	56.478 ± 0.04	79.168 ± 0.02	183.259 ± 0.01
400	80.17 ± 0.1	70.83 ± 0.2	55.68 ± 0.04	42.65 ± 0.04	34.38 ± 0.2	4.251 ± 0.4	17.730 ± 0.08	45.009 ± 0.5	66.583 ± 0.05	151.889 ± 0.2
600	85.42 ± 0.2	74.98 ± 0.01	65.43 ± 0.02	48.37 ± 0.1	41.16 ± 0.4	3.099 ± 0.8	15.188 ± 0.04	35.089 ± 0.2	59.949 ± 0.01	136.204 ± 0.05
800	90.37 ± 0.5	80.33 ± 0.5	75.36 ± 0.01	57.34 ± 0.1	50.66 ± 0.02	2.042 ± 0.06	11.965 ± 0.05	25.108 ± 0.2	49.534 ± 0.2	114.196 ± 0.05
1000	91.83 ± 0.04	87.98 ± 0.04	79.03 ± 0.02	65.72 ± 0.5	58.70 ± 0.5	1.735 ± 0.05	6.137 ± 0.05	21.326 ± 0.1	39.801 ± 0.5	95.597 ± 0.2

Table 3 Impact of duration of immersion on mild steel corrosion inhibition in 1 N HCl, both with and without the optimal CVLE content (1000 ppm) at 298 K

Immersion time (h)	Loss of weight without CVLE	Loss of weight in the presence of CVLE	%IE in the presence of CVLE
12	0.0392 ± 0.004	0.0076 ± 0.001	80.6122 ± 0.01
24	0.1387 ± 0.002	0.0174 ± 0.002	87.4549 ± 0.01
36	0.1956 ± 0.005	0.0328 ± 0.002	83.3078 ± 0.05

Table 4 Thermodynamic and kinetic parameters of mild steel in 1 N HCl in the without and with CVLE

Concentration (ppm)	E_a (kJ mol^{-1})	ΔH_a (kJ mol^{-1})	ΔS_a (kJ mol^{-1})
Blank	45.6931	43.0566	−72.9343
200	69.0209	66.3843	−5.2298
400	71.3986	68.7620	0.32858
600	75.3070	72.6704	11.0864
800	79.7632	77.1266	22.8655
1000	83.1220	80.4854	31.1332

Fig. 5 plots the natural logarithm of C_R *vs.* $1/T$ for mild steel corrosion in a 1 N HCl solution with and without different CVLE concentrations. The slope ($-E_a/2.303R$) of the lines could be utilized to calculate the activation energy (E_a). As per Table 4, the E_a values for 1 N HCl solutions with inhibitors range from 69.0209 ± 0.01 to 83.1220 ± 0.4 kJ mol^{-1}, and are greater than those without CVLE. This demonstrates unequivocally that the concentration of CVLE raises the energy barrier of the corrosion reaction.[43] Furthermore, to comply with physical adsorption, activation energy between 40 and 80 kJ mol^{-1} can be suggested. A transition state plots $\log C_R/T$ *vs.* $1/T$ (Fig. 6) to further understand these findings. The graph's slope ($-\Delta H_a/2.303RT$) yielded straight lines, and the intercept ($\log R/Nh + \Delta S_a/2.303R$) was computed to process the activation enthalpy (ΔH_a) and activation entropy (ΔS_a) values in Table 4, respectively. The mild steel dissolution phenomenon is endothermic, meaning that mild steel is difficult to dissolve, as indicated by the positive value of ΔH_a. Besides, the entropy of adsorption (ΔS_a) increases with increasing CVLE concentrations. The positive value of ΔS_a towards higher CVLE concentration (1000 ppm) was observed in 1 N HCl medium. This shows that the process is less orderly to a more random arrangement.[44]

3.3 Adsorption studies

The adsorption isotherm may provide details on the inhibitor molecules thought to bind on the metallic substrate and prevent corrosion. Several isotherm models, including the Langmuir, Freundlich, and Temkin models shown in Fig. 7, can be used to explain the adsorption process. The following eqn (15)–(17) can be used to represent their expressions:[25]

Langmuir:

$$C_{inh}/\theta = 1/K_{ads} + C_{inh} \quad (15)$$

Freundlich:

$$\log \theta = n \log C_{inh} + \log K_{ads} \quad (16)$$

Temkin:

$$\theta = -1/2a \ln K_{ads} - 1/2a \ln C_{inh} \quad (17)$$

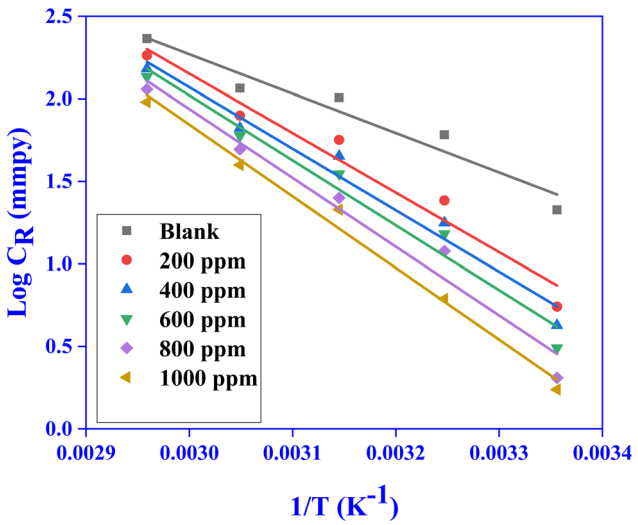

Fig. 5 Arrhenius plots with and without different CVLE concentrations in 1 N HCl medium.

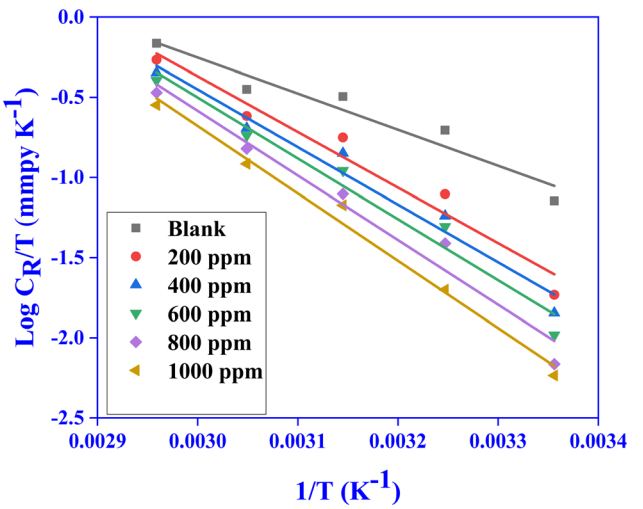

Fig. 6 Transition state plots with and without different CVLE concentrations in 1 N HCl medium.

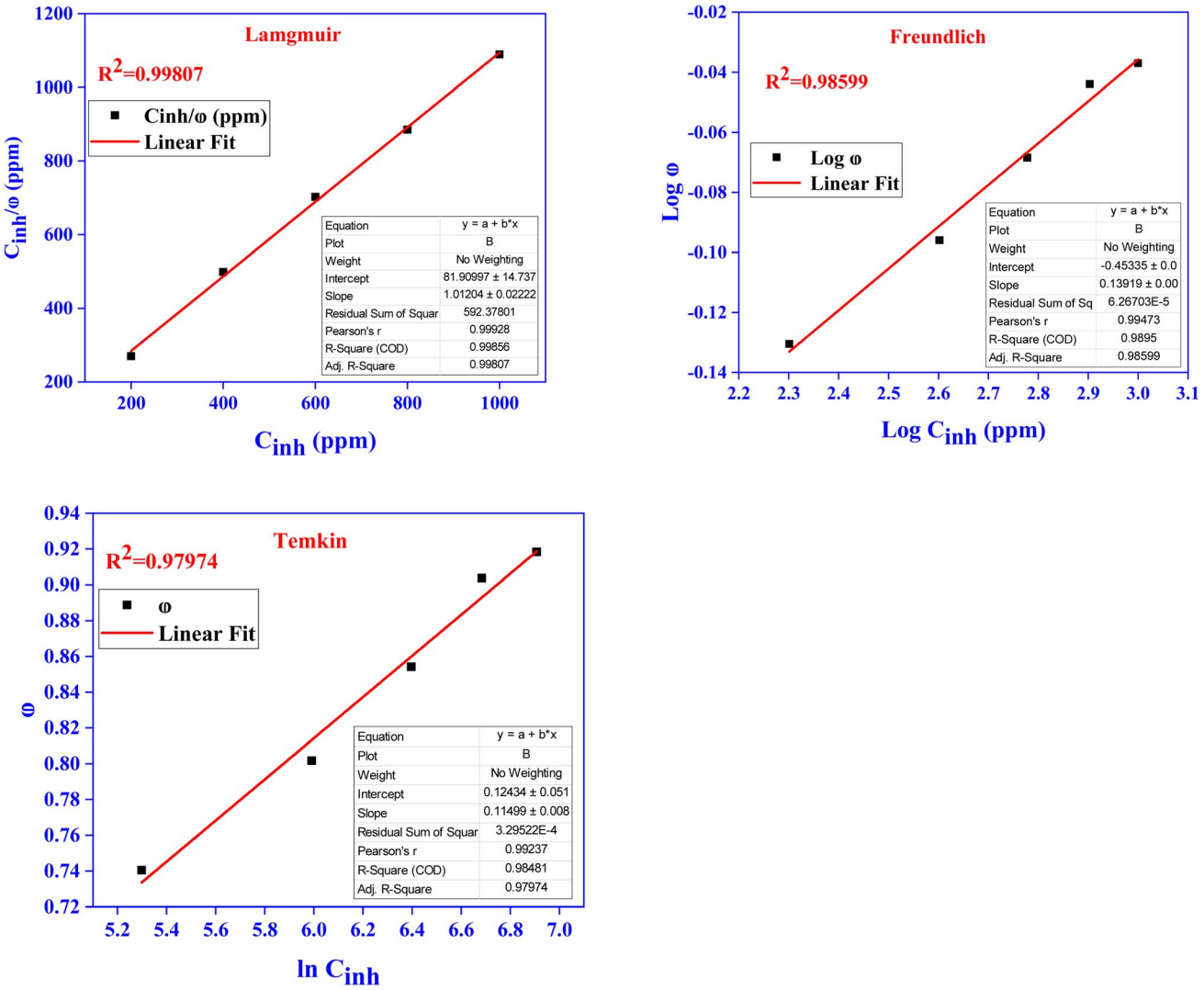

Fig. 7 Various adsorption isotherms of CVLE over mild steel in 1 N HCl.

here, θ stands for surface coverage, K_{ads} for adsorption equilibrium constant, and C_{inh} for inhibitor concentration.

After analyzing the data, the Langmuir adsorption isotherm was discovered to fit the data very well, with a regression coefficient (R^2) of 0.99807 ± 0.001, which is <1 for the straight lines depicted in Fig. 8. This indicates that the model provides an excellent representation of the adsorption process.

According to the experimental result, the Langmuir model accurately depicts how CVLE adsorbs on the substrate of the adsorbent, and the model's presumptions appear to be suitable in this case. To calculate the adsorption equilibrium constant (K_{ads}), we used eqn (15), which involves the reciprocal of the intercept from a linear plot. Additionally, eqn (18) was used to correlate K_{ads} to ΔG°_{ads} (standard free energy of adsorption).[26]

$$\Delta G^{\circ}_{ads} = -RT \ln(55.5 K_{ads}) \quad (18)$$

where the molar water temperature is T, the universal gas constant is R, and the concentration is 55.5 mol L^{-1}.

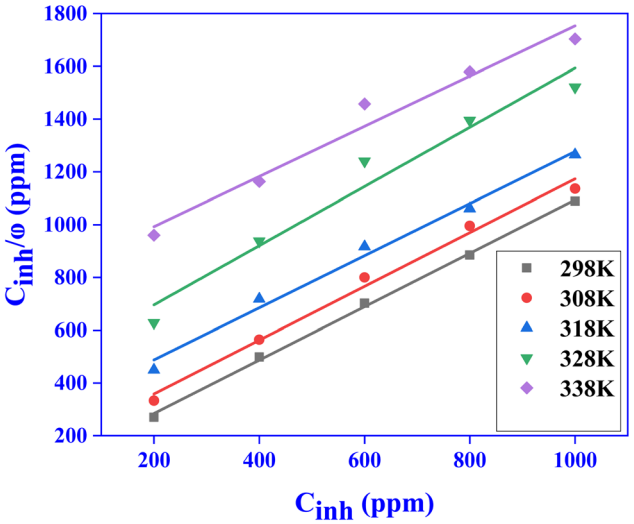

Fig. 8 Langmuir adsorption isotherms at various temperatures.

Table 5 Parameters for thermodynamic adsorption of CVLE at numerous temperatures

Temperature (K)	K_{ads}	R^2	Slope	ΔG°_{ads} (kJ mol^{-1})
298	12208.526 ± 4.2	0.99807 ± 0.001	1.01204 ± 0.002	−33.2705 ± 0.02
308	6471.367 ± 2.8	0.98769 ± 0.001	1.01926 ± 0.001	−32.7613 ± 0.04
318	3445.205 ± 1.4	0.98577 ± 0.004	0.98699 ± 0.002	−32.158 ± 0.04
328	2120.046 ± 1.5	0.94938 ± 0.002	1.12173 ± 0.004	−31.8449 ± 0.02
338	1246.797 ± 2.2	0.95949 ± 0.005	0.95127 ± 0.005	−31.3238 ± 0.05

Table 5 demonstrates that the values of K_{ads} drop with increasing temperature, suggesting that the contacts across the substrate and the adsorbed CVLE molecules weaken. It means that the inhibitor molecules are more likely to separate from the surface and when the temperature rises, protective effectiveness decreases. Physical adsorption is the driving force behind the spontaneous adsorption of CVLE onto the mild steel surface, as indicated by the negative values of ΔG°_{ads}. ΔG°_{ads} values are below −40 kJ mol^{-1} and fall between −31.3238 ± 0.05 and −33.2705 ± 0.02 kJ mol^{-1}, supporting the idea that the adsorption process is physical.[27]

3.4 Electrochemical measurements

3.4.1 Open circuit potential (OCP). A stable OCP must be achieved prior to doing EIS and PDP studies. To put it another way, the electrode should be given time to stabilize in a state where the potential does not change much over time. In contrast to temporary effects or fluctuations, this guarantees that the measurements made during PDP and EIS are precise and represent the system's actual electrochemical behavior. During each concentration gradient experiment, the mild steel coupon which served as the working electrode, was immersed in the test solution for an hour. The OCP *vs.* time curves (in seconds) are displayed in Fig. 9 both with and without the addition of different CVLE concentrations ranging from 200 ppm to 1000 ppm.[45] In comparison to the blank, the open circuit potential (E_{OCP}) becomes more positive at lower inhibitor concentrations and more negative at higher concentrations, as illustrated in Fig. 9. This implies that mixed-type inhibition was shown by CVLE.[46]

3.4.2 Potentiodynamic polarization (PDP) analysis. The Tafel graphs for MS in 1 N HCl solutions with the increase of various CVLE doses in Fig. 10 illustrate the potentiodynamic polarization data. These curves provided the corrosion kinetic parameters, which are listed in Table 6 and include E_{corr}, I_{corr}, and the anodic and cathodic Tafel slopes (β_a and β_c). Eqn (19) was used to calculate the values of %IE.[47]

$$\%IE = \frac{I^0_{corr} - I^0_{inh}}{I^0_{corr}} \times 100 \quad (19)$$

where I^0_{corr} and I^0_{inh} denotes the corrosion current density in the availability and unavailability of inhibitor.

Table 6 clearly demonstrates a progressive decline in corrosion current density (I_{corr}) with increasing concentrations of CVLE, decreasing from 157.63 ± 0.01 μA cm^{-2} for the uninhibited blank solution to 4.02 ± 0.02 μA cm^{-2} at 1000 ppm, corresponding to a high inhibition efficiency (IE%) of 97.44 ± 0.02%. This significant reduction in i_{corr} highlights the potent inhibitive action of CVLE on the electrochemical dissolution of mild steel in 1.0 N HCl. An anodic shift in the corrosion potential (E_{corr}) was observed, moving from −408.7 ± 0.2 mV

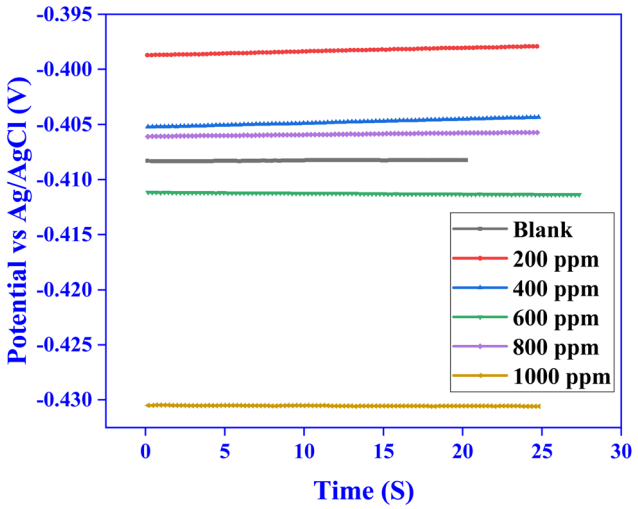

Fig. 9 OCP of mild steel with and without CVLE at various concentrations.

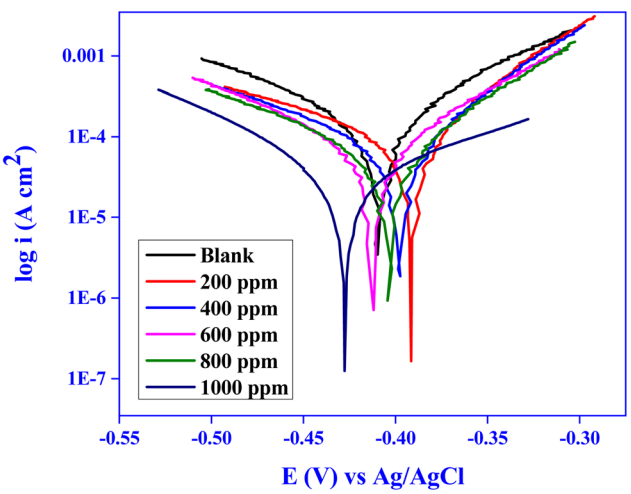

Fig. 10 Tafel curves for mild steel with and without CVLE at various concentrations.

Table 6 Polarisation characteristics of mild steel samples with and without varying CVLE concentrations

Conc. (ppm)	β_a (mV per dec)	$-\beta_c$ (mV per dec)	E_{corr} (mV)	i_{corr} (μA cm^{-2})	C_R (mmpy)	R_p (Ω)	IE (%)	θ
Blank	129.70 ± 0.02	108.24 ± 0.05	−408.7 ± 0.2	157.63 ± 0.01	1.831 ± 0.05	162.56 ± 0.02	—	—
200	120.33 ± 0.05	94.46 ± 0.01	−413.2 ± 0.5	103.18 ± 0.2	1.347 ± 0.05	274.13 ± 0.02	34.54 ± 0.04	0.3454 ± 0.04
400	110.75 ± 0.04	74.75 ± 0.01	−410.6 ± 0.1	94.58 ± 0.05	1.009 ± 0.04	282.37 ± 0.01	39.99 ± 0.03	0.3999 ± 0.03
600	105.51 ± 0.01	60.78 ± 0.02	−404.8 ± 0.2	55.47 ± 0.02	0.644 ± 0.06	290.00 ± 0.01	64.80 ± 0.05	0.6480 ± 0.05
800	62.31 ± 0.02	88.40 ± 0.05	−399.3 ± 0.6	53.47 ± 0.01	0.617 ± 0.01	300.92 ± 0.05	66.07 ± 0.02	0.6607 ± 0.02
1000	8.20 ± 0.02	7.93 ± 0.02	−392.8 ± 0.2	4.02 ± 0.02	0.0621 ± 0.05	331.83 ± 0.02	97.44 ± 0.02	0.9744 ± 0.02

(blank) to −392.8 ± 0.2 mV at 1000 ppm, suggesting that CVLE primarily affects the anodic reaction pathway. This conclusion is further supported by the marked reduction in the anodic Tafel slope (β_a), which decreased from 129.70 ± 0.02 mV per decade for the blank to 8.20 ± 0.02 mV per decade at the highest inhibitor concentration. Such a significant decrease indicates substantial suppression of the anodic metal dissolution process.[48] In contrast, the cathodic Tafel slope (β_c) exhibited a more moderate decrease, suggesting that the inhibitor also impedes the cathodic hydrogen evolution reaction, but to a lesser extent. This dual influence implies that CVLE acts as a mixed-type inhibitor with dominant anodic inhibition behavior. Additionally, the polarization resistance (R_p) values showed a consistent increase with higher inhibitor concentrations, reinforcing the conclusion that the protective film formed by CVLE improves the resistance of the metal–electrolyte interface to charge transfer. The combined electrochemical parameters confirm that CVLE effectively inhibits mild steel corrosion by adsorbing onto active sites, primarily blocking anodic dissolution and forming a stable protective barrier.

3.4.3 Electrochemical impedance spectroscopy (EIS) analysis. The corrosion behavior of mild steel (MS) in a 1.0 N HCl media was analyzed using EIS, both with and without varying concentrations of CVLE. The outcomes of these studies are depicted in the Nyquist and Bode plots, which are displayed in Fig. 11 and 12, respectively.[45] As can be seen in Fig. 11, the diameter of each semicircle of the Nyquist plot gradually increased as the concentration of CVLE inhibitors increased from 200 to 1000 ppm.[49] At the greatest concentration of 1000 ppm, as is evident in Fig. 12(a), the R_{ct} values were likewise increased from 21.569 ± 0.1 to 635.121 ± 0.1 ohm cm^2 due to the arrangement and persistent rise in the conservativeness of the boundary layer of the inhibitive particles (IE 96.6039 ± 0.04%) adsorbed. Consequently, MS's corrosion rates were

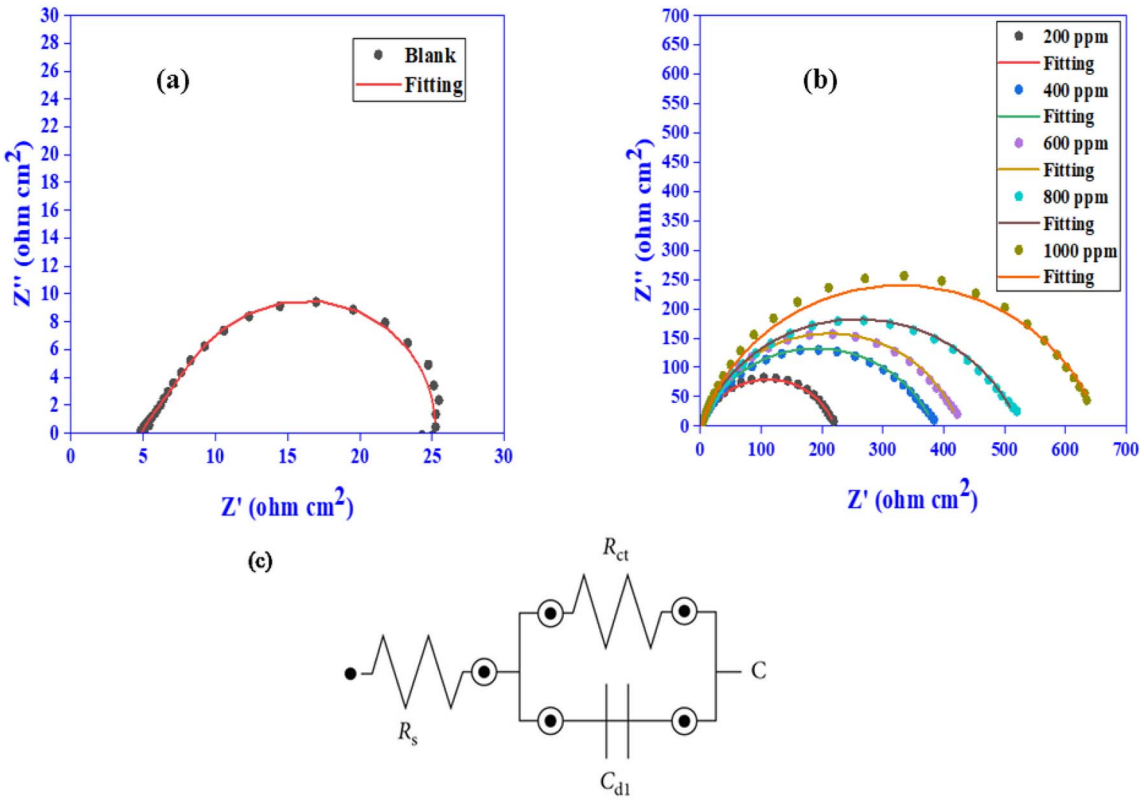

Fig. 11 Nyquist plots for MS in 1.0 N HCl solution (a) without and (b) with varying CVLE concentrations; (c) equivalent circuit diagram.

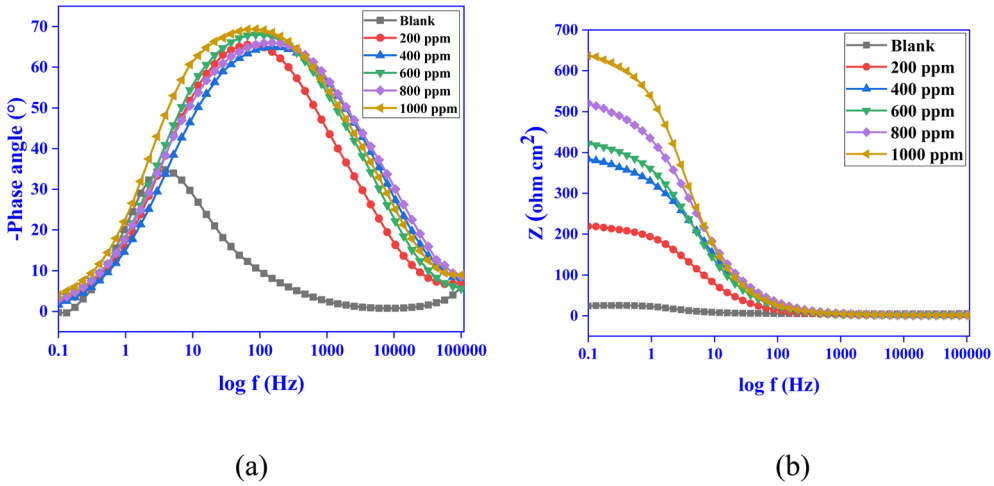

Fig. 12 (a) Plots of Bode phase (phase angle against log *f*) and (b) plots of Bode modulus (*Z vs.* log *f*).

continuously decreased. Table 7 presents key electrochemical impedance parameters, including inhibition efficiency (IE%), double-layer capacitance (C_{dl}), solution resistance (R_s), and charge transfer resistance (R_{ct}). A notable and consistent decrease in C_{dl} values, from 1075.21 ± 0.01 to 85.07 ± 0.4 μF cm^{-2}, was observed as the concentration of CVLE increased from 200 to 1000 ppm. This substantial reduction in C_{dl} signifies the effective adsorption of CVLE molecules onto the mild steel surface, which leads to the formation of a protective layer that minimizes surface roughness and dielectric constant at the metal–electrolyte interface. The decline in capacitance reflects the displacement of water molecules and corrosive ions by organic constituents of the inhibitor, thereby decreasing the system's ability to store charge and impeding corrosion processes. Although the open circuit potential (OCP) at 1000 ppm shows a slightly more negative shift compared to the blank, this should not be interpreted as reduced protection. On the contrary, the dramatic increase in R_{ct} from 21.57 to 635.12 Ω cm^2 clearly indicates enhanced corrosion resistance due to the formation of a dense and stable inhibitive film.[50,51] This apparent discrepancy can be attributed to the mixed-type inhibitory nature of CVLE. At higher concentrations, the extract appears to suppress the cathodic hydrogen evolution reaction more dominantly, leading to a negative shift in OCP, while still effectively inhibiting both anodic and cathodic processes overall. Thus, the combined impedance and polarization data validate the strong adsorption and protective efficiency of CVLE even at its highest tested concentration. Eqn (20) was used to calculate inhibition efficiency (IE%) from EIS data in the manner described below.

$$E_R(\%) = \frac{R_{ct}^{inh} - R_{ct}^{0}}{R_{ct}^{inh}} \times 100 \quad (20)$$

The charge transfer resistance values with and without an inhibitor are represented by R_{ct}^{0} and R_{ct}^{inh}, respectively.

Eqn (21) and the frequency (f_{max}) at which the imaginary component of the impedance is maximum – $Z_{im(max)}$ – were used to compute the C_{dl} values.

$$C_{dl} = \frac{1}{2\pi f_{max} R_{ct}} \quad (21)$$

3.5 Surface analysis

3.5.1 Scanning electron microscopy. Scanning electron microscopy (SEM) was used to analyze the surface morphologies of mild steel (MS) following three hours of dipping in a 1 N HCl media at 298 K. Fig. 13(a)–(c) display the SEM images of mild steel surfaces before immersion, after immersion in 1 N HCl and with CVLE inhibitor respectively. Following immersion, the mild steel that was immersed in a 1 NHCl solution showed

Table 7 Impedance measurements at room temperature with and without different inhibitor doses

Conc. (in ppm)	R_s (Ω cm^2)	R_{ct} (Ω cm^2)	f_{max} (Hz)	C_{dl} (μF cm^{-2})	IE (%)	θ
Blank	5.3934 ± 0.01	21.569 ± 0.1	6.8665 ± 0.001	1075.2128 ± 0.01	—	—
200	1.2963 ± 0.05	218.952 ± 0.2	3.9069 ± 0.001	186.1483 ± 0.2	90.1621 ± 0.1	0.9016 ± 0.1
400	1.3563 ± 0.01	383.843 ± 0.4	2.9471 ± 0.001	140.7641 ± 0.05	94.3807 ± 0.02	0.9438 ± 0.02
600	1.3614 ± 0.1	421.903 ± 0.2	2.9471 ± 0.001	128.0657 ± 0.5	94.8876 ± 0.05	0.9488 ± 0.05
800	1.3539 ± 0.02	520.192 ± 0.4	2.9471 ± 0.001	103.7392 ± 0.2	95.8536 ± 0.2	0.9585 ± 0.2
1000	1.3521 ± 0.05	635.121 ± 0.1	2.9471 ± 0.001	85.07246 ± 0.4	96.6039 ± 0.04	0.9660 ± 0.04

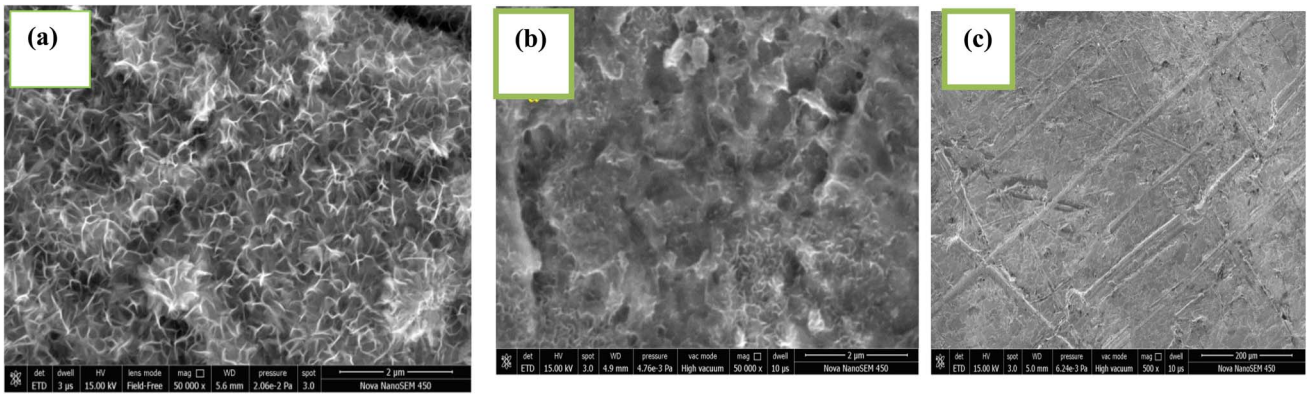

Fig. 13 SEM images of mild steel sample (a) before immersion, (b) after immersion in an acidic medium without inhibitor, (c) with CVLE (1000 ppm).

significant surface damage, as illustrated in Fig. 13(b), which also demonstrated that the surface was severely corroded.[51,52] In a vigorous hydrochloric solution, it can be inferred that the MS surface is severely eroded. Strong acidic liquids are frequently the site of this corrosion. After 1000 ppm of inhibitor is added to a 1 N HCl solution, a mild steel surface that is smooth and covered in inhibitor deposits is shown in Fig. 13(c). SEM photos clearly show that the inhibited surface is missing the surface irregularities caused by corrosion, and the surface is currently essentially free of corrosion.[53]

3.5.2 EDS studies. Before and after a three-hour immersion, the composition of mild steel was examined using EDS. The EDS spectrum in Fig. 14(a) shows that, in the absence of the inhibitor, the mild steel surface is composed of 15.58% oxygen (O) and 73.23% iron (Fe) by weight. But when the CVLE is added, the composition shifts to 81.75 percent iron and 5.02% oxygen, as Fig. 14(b) illustrates. The mild steel sample submerged in 1 N HCl with 1000 ppm CVLE showed a reduced oxygen content, which may indicate that the inhibitor creates a defensive coating upon the metallic surface.[54] The elements iron (Fe), carbon (C), and oxygen (O) were found on the surface of the mild steel, as shown in Fig. 14. The proportion of carbon on the metal surface elevated when the CVLE extract was added to the 1 N HCl solution, which reveal the emergence of a defensive layer based and decrease in rate of corrosion.[55]

3.5.3 XPS analysis. For the analysis of metal surfaces, X-ray photoelectron spectroscopy (XPS) is a thorough approach. This technique is used to ascertain the electronic structure of the compounds, the chemical state of the elements present, and the elemental makeup of a surface. In this case, the atomic binding

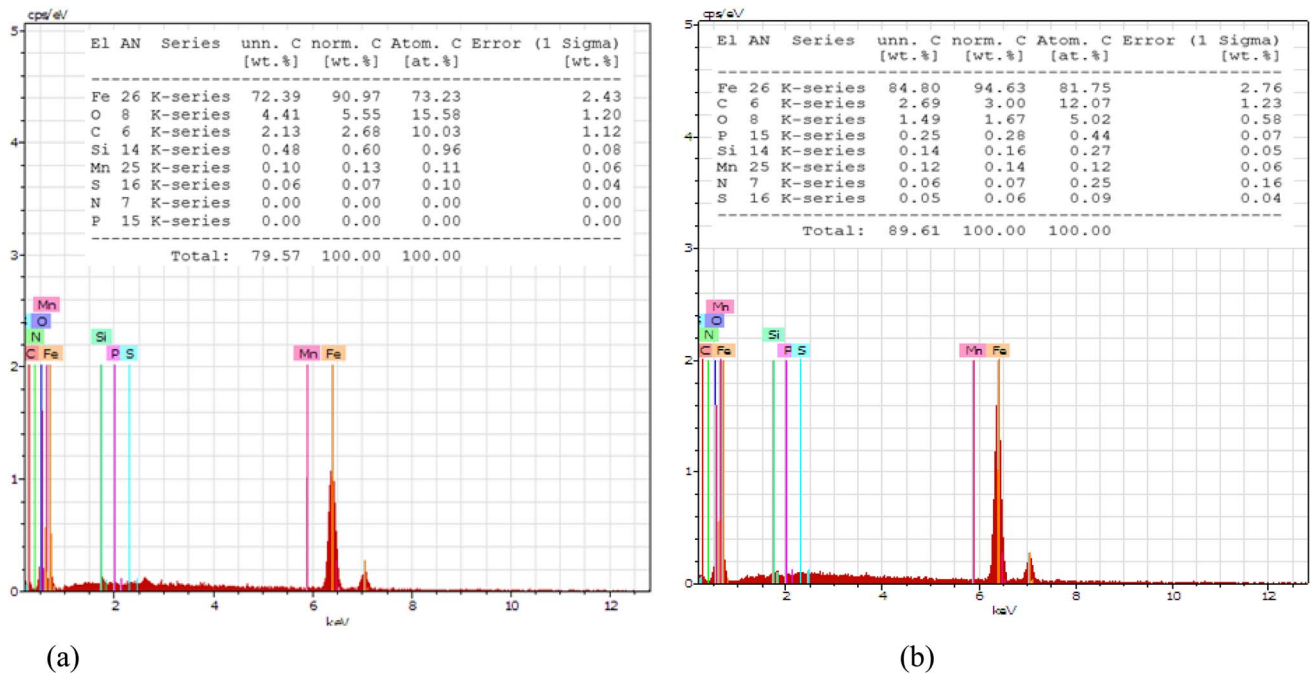

Fig. 14 EDS spectra of mild steel (a) immersion in 1 N HCl and (b) immersion in CVLE (1000 ppm) at 298 K.

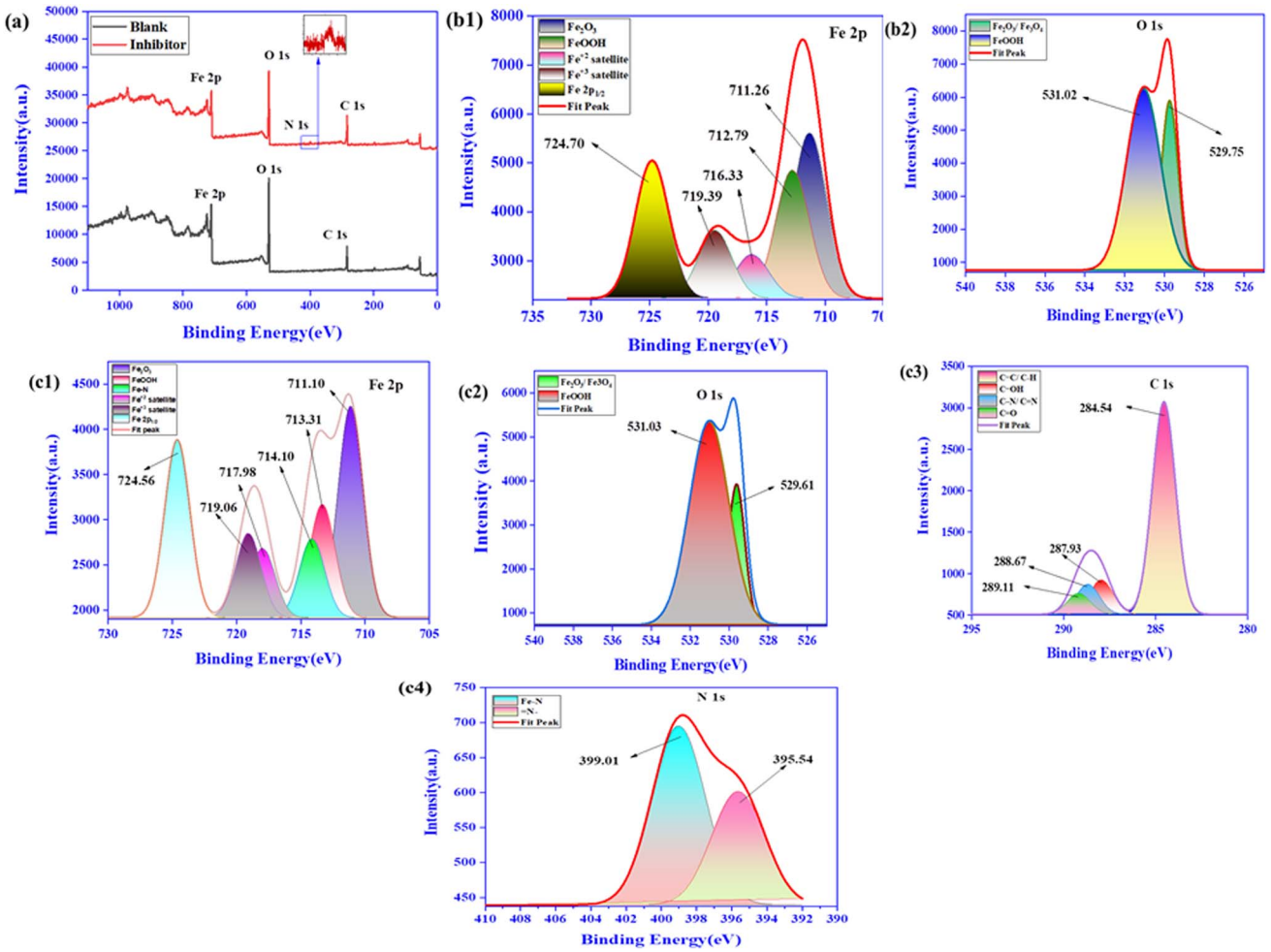

Fig. 15 (a) XPS survey graph of mild steel with and without CVLE (1000 ppm) in 1 N HCl, (b1 and b2) XPS deconvoluted profiles without and (c1–c4) with CVLE in 1 N HCl on mild steel.

energies of elements including carbon, nitrogen, oxygen, and iron were ascertained using XPS.[13]

The existence of Fe^{2+} and Fe^{3+} species is indicated by the Fe 2p spectra (Fig. 15(b1) and (c1)), which shows satellite peaks at 717.98 eV and 719.06 eV in addition to two peaks at about 711.10 eV (Fe $2p^{3/2}$) and 724.56 eV (Fe $2p^{1/2}$). Two distinct components at 711.10 eV and 713.31 eV, which correspond to Fe_2O_3 and FeOOH, respectively, are revealed by further deconvolution of the Fe $2p^{3/2}$ peak. An additional peak that corresponds to the Fe–N bond is seen at 714.10 eV when Fig. 15(b1) and (c1) are compared. This peak indicates that the CVLE inhibitor has been adsorbed onto the mild steel surface, confirming its presence there. The existence of Fe_2O_3/Fe_3O_4 and FeOOH is indicated by two peaks in the O 1 s spectrum seen in Fig. 15(b2) and (c2) at 529.61 eV and 531.03 eV, respectively.[56]

Following deconvolution, the CVLE C 1s spectra displays four peaks at 284.54, 287.93, 288.67, and 289.11 eV (Fig. 15(c3)). The contaminating hydrocarbon and the C–C, C=C, and C–H bonds are responsible for the first peak; the C–OH bond may be the primary cause of the second peak; the existence of C–N/C=N bonds may be indicated by the third peak; and the C=O bond[57] is responsible for the fourth peak. This attests to CVLE's successful adsorption on mild steel surfaces. Furthermore, two peaks at 395.54 eV and 399.01 eV are visible in the N 1s spectra (Fig. 15(c4)), which correspond to the Fe–N and =N groups, respectively. These synergistic corrosion inhibitors substantially enhance the creation of a protective adsorption film since it is clear from the preceding data that atoms from the CVLE molecules interact with the mild steel surface through bonding.[57]

3.6 FTIR studies

By improving the inhibitor molecule's adsorption on the metallic substrate, the inclusion of the aromatic ring and heteroatoms (O) may reduce corrosion. The FTIR spectra of the CVLE extract are displayed in Fig. 16. The C–N stretching vibration peak is located at 1000 cm^{-1} in the FTIR spectra of the CVLE extract.[58] At 2965 cm^{-1}, a C–H vibration peak was observed. The C–O stretching is responsible for the peak at 1065 cm^{-1}. The C=O bond is attributed to the peak at 1720 cm^{-1}. The presence of a methyl group in the extract is shown by the $-CH_3$ band at 1400 cm^{-1}. The distinctive vibrations of the methylene group ($-CH_2$) are observed at

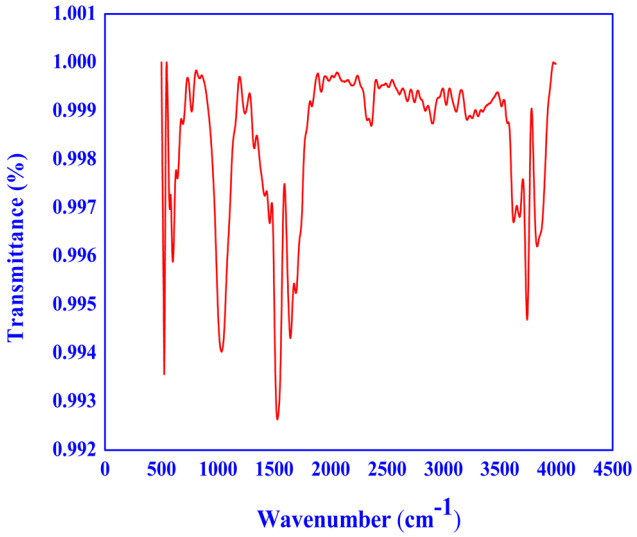

Fig. 16 FTIR spectra of CVLE extract.

1500 cm^{-1}.[59] The OH stretching vibration zone, which is most frequently observed in compounds including alcohols, phenols, and carboxylic acids, usually falls between the 3500–4000 cm^{-1} range. Because of the hydroxyl group's hydrogen bonding interactions, these molecules show a broad and strong absorption band in this region.

3.7 DFT analysis

Fig. 17 illustrates the electrical characteristics and optimized geometries of glaucine, oxoglaucine, and ellagic acid molecules. These visual representations provide insights into the spatial distribution of the HOMO and LUMO across the molecular structures. The analysis reveals a relatively uniform distribution of these orbitals across the molecular framework, suggesting extensive charge delocalization. This uniformity implies that electrons are shared rather than restricted to particular areas among multiple atoms within the molecules.[60] The observed charge-sharing behavior is enhanced by the presence of heteroatoms and aromatic rings in the molecular structures. Heteroatoms contribute more electronic configurations, whereas aromatic rings promote electron delocalization through resonance, collectively enhancing the electronic and chemical properties of these compounds. As a result, glaucine, oxoglaucine, and ellagic acid demonstrate significant charge distribution, which plays a critical role in their reactivity and electronic behavior in various chemical environments.

Fig. 18 presents Electrostatic Potential Surface (ESP) maps, which offer a visual representation of molecular polarity and are invaluable for understanding the corrosion inhibition process. These maps highlight regions of negative electrostatic potential (depicted in red), which are more susceptible to nucleophilic attacks, and areas of positive electrostatic potential (depicted in blue), which are more prone to electrophilic attacks. Typically,

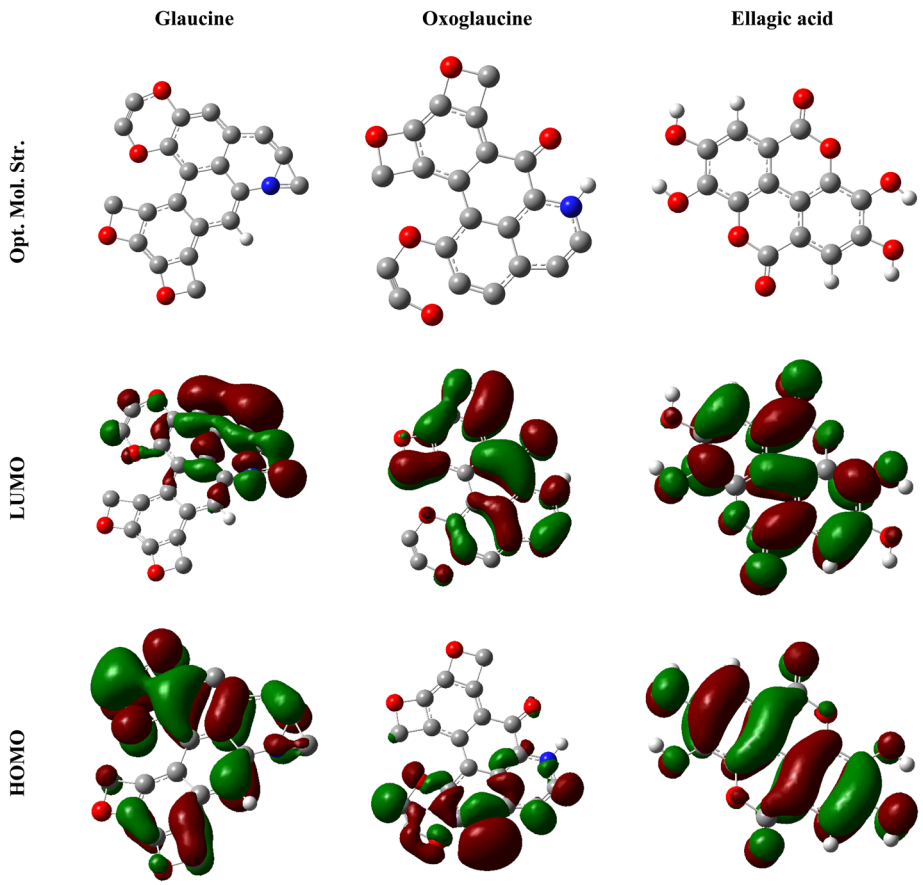

Fig. 17 Optimized geometries and FMOs of the glaucine, oxoglaucine and ellagic acid.

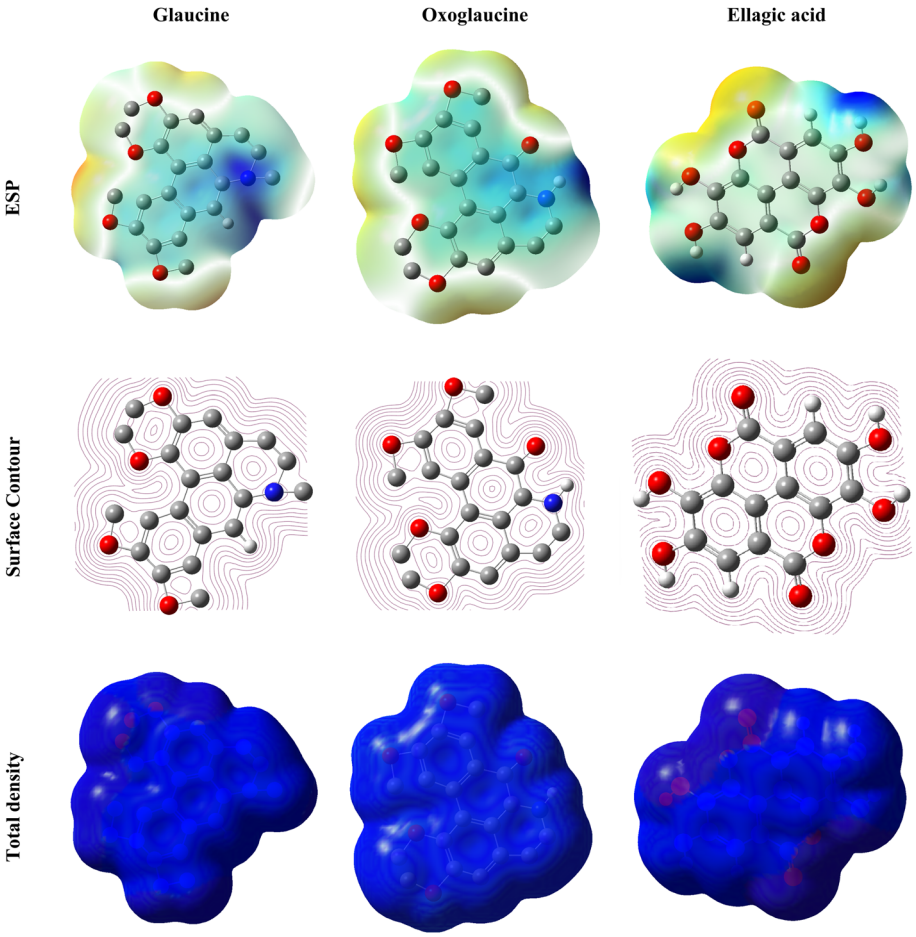

Fig. 18 Depiction of the ESP, surface contour and total density of the glaucine, oxoglaucine and ellagic acid.

negative potential regions heteroatoms like oxygen, which readily form covalent connections with metal atoms, are surrounded by concentrated areas, as shown in Fig. 18. In contrast, electrophilic interactions are directed towards positive potential sites, which are frequently connected to hydrogen and carbon atoms.[61] The analysis of these ESP maps reveals that compounds like glaucine, oxoglaucine, and ellagic acid possess notable anti-corrosive properties. Their effectiveness in mitigating corrosion is attributed to their capacity to engage with metal surfaces and create protective films that prevent exposure to agents that cause corrosion. Their adsorption onto metal surfaces is greatly improved by functional groups such as conjugated double bonds and phenolic hydroxyl groups, facilitating the formation of stable passivation layers. These features make these molecules highly effective corrosion inhibitors, demonstrating their potential for widespread use in industrial applications due to their strong anti-corrosive performance and compatibility with metal substrates.[62]

In the study of corrosion inhibition for mild steel in 1 M HCl, various electronic parameters are pivotal in understanding the efficiency of potential inhibitors, as summarized in Table 8. The values of the E_{HOMO} and E_{LUMO} provide key insights into the electron-donating and electron-accepting abilities of the inhibitors. For example, glaucine has an E_{HOMO} of −0.24064 eV and an E_{LUMO} of −0.18580 eV, highlighting its strong electron-donating capacity along with the potential to accept electrons. The ΔE between E_{HOMO} and E_{LUMO} is another critical parameter that reflects molecular reactivity and stability. Glaucine and oxoglaucine exhibit ΔE values of 0.05484 eV and 0.04733 eV, respectively, indicating higher reactivity compared to ellagic acid, which has a larger ΔE of 0.15498 eV. Additional

Table 8 Using the DNP 3.5 basis set and the GGA/BLYP approach, pertinent electronic characteristics about the extract components in the aqueous phase

Code	Glaucine	Oxoglaucine	Ellagic acid
Basis set	DNP	DNP	DNP
Function	GGA	GGA	GGA
E_{HOMO} (ev)	−0.24064	−0.23430	−0.24063
E_{LUMO} (ev)	−0.18580	−0.18697	−0.08565
ΔE (eV)	0.05484	0.04733	0.15498
IP (eV)	0.0.24064	0.23430	0.24063
EA (eV)	0.18580	0.18697	0.08565
χ (eV)	0.21322	0.210635	0.16314
η (eV)	0.02742	0.023665	0.07749
Σ	36.46973012	42.25649694	120.90489095
ΔN(Fe) (e)	0.066586	0.057498	0.190116

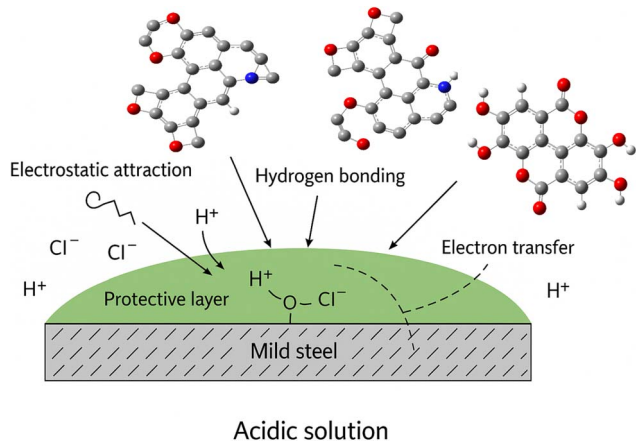

Fig. 19 Depiction of the adsorption of glaucine, oxoglaucine and ellagic acid on mild steel.

parameters, such as IP and EA, provide further details about molecular stability and electron affinity. Ellagic acid shows an IP of 0.24063 eV and an EA of 0.08565 eV, signifying both stability and an ability to attract electrons. χ highlights the tendency of molecules to attract electrons, with glaucine having the highest χ value of 0.21322 eV, followed by oxoglaucine (0.210635 eV) and ellagic acid (0.16314 eV).

η indicative of molecular stability, is highest for ellagic acid at 0.07749 eV, suggesting its greater resistance to deformation compared to the other inhibitors. Conversely, σ and the fraction of electron transfer to the Fe surface (ΔN(Fe)) reveal the molecules' ability to interact with the metal surface and form protective layers. Ellagic acid demonstrates the highest values for σ and ΔN(Fe), emphasizing its potential as a highly effective corrosion inhibitor in acidic environments.[63]

4. Mechanism of mitigation

Glaucine, oxoglaucine, and ellagic acid are examples of compounds that inhibit mild steel corrosion in 1 M HCl by a multi-step process. These molecules first adsorb onto the metal surface through a variety of interactions, including electrostatic attractions, hydrogen bonds, and van der Waals forces.[64] After being absorbed, they cover the metal in a protective coating that serves as a barrier against corrosive substances like the acidic solution's H^+ and Cl^- ions. By preventing direct contact between the corrosive species and the metal surface, this protective layer inhibits corrosion.[65] Additionally, the inhibitor molecules donate electrons to the metal or form coordination bonds with metal ions in electron transfer interactions with the metal surface. This contact slows down the corrosion process and lessens the metal surface's reactivity. In order to prevent corrosive species in the solution, like dissolved oxygen or H^+ ions, from reacting with the metal, the inhibitor molecules may also interact with them.[66] To further reduce corrosion, this interaction may entail the scavenging of free radicals or the creation of stable complexes. Furthermore, inhibitor molecules change the metal's surface chemistry, resulting in the development of passive layers or surface complexes that are less likely to corrode. These changes guarantee the metal component's continued integrity by offering long-term corrosion prevention.[67] It could be stated that the corrosion inhibition mechanism of these molecules involves a combination of adsorption, formation of protective layers, electron transfer reactions, reduction of corrosive species, modification of surface chemistry, and continuous protection, collectively mitigating mild steel corrosion in acidic environments like 1 N HCl.[68] Fig. 19 shows the adsorption of glaucine, oxoglaucine and ellagic acid on mild steel.

Table 9 Comparative analysis of corrosion inhibition efficiency of CVLE with other reported plant extracts

Inhibitor	Testing conditions	Inhibitors concentration	Efficiency (%)	Type of inhibitor	Ref.
Prickly pear no pales pulp (PPUN)	XC38 steel, 1 M HCl	25 ppm	WL: 83.00 PDP: 93.22 EIS: 96.00	Mixed	13
Alysicarpus compactum extract	St37 carbon steel, 1 M HCl	0.4 g L^{-1}	WL: 85.48 PDP: 79.06 EIS: 80.28	Mixed	16
Senggani (*Melastoma candidum D. Don*) leaf extract	St-37 steel, 1 N HCl	0.8%	WL: 67.00 PDP: 69.72	Mixed	69
Schinopsis lorentzill extract	Carbon steel, 1 M HCl	2000 ppm	PDP: 66.00 EIS: 38.60	Mixed	70
Haematostaphis barteri leaves extract	Mild steel, 1 M HCl	40 g L^{-1}	WL: 73.74	Mixed	71
Thymus vulgaris plant extract	304 stainless steel, 1 M HCl	2%	PDP: 49.00 EIS: 62.15	Mixed	72
Elaeis guineensis extract	Mild steel, 1 M HCl	10% (v/v)	WL: 73.81	—	73
Cynara cardunculus leaves extract	St37 steel, 15% H_2SO_4	30 ppm	WL: 80.60 PDP: 69.40 EIS: 78.15	Mixed	74
Ammophila arenaria extract	Mild steel, 1 M HCl	700 ppm	PDP: 83.67 EIS: 84.32	Mixed	75
Codiaeum variegatum leaves extract	Mild steel, 1 N HCl	1000 ppm	WL: 91.83 PDP: 97.44 EIS: 96.60	Mixed-type	Present work

4.1 Comparative analysis

The performance of CVLE extract as a corrosion inhibitor was compared to that of other plant extract inhibitors mentioned in the published research in order to assess its efficacy. The efficiency of inhibition, concentrations, metal types, electrolytes, and methods for several natural inhibitors are compiled in Table 9. With an inhibitory efficacy of 97.44%, CVLE extract performs well in comparison to other plant-based inhibitors. These findings place CVLE extract competitively within the range of natural inhibitors and demonstrate its efficacy as a strong corrosion inhibitor. The thorough comparison highlights CVLE extract's potential for real-world corrosion prevention applications, especially considering its efficiency and concentration requirements. As a result, this comparison study supports the significance of CVLE extract as a natural inhibitor that works well and has positive environmental effects, supporting the continuous advancement of long-term corrosion prevention techniques.

5. Conclusion

• The mild steel's corrosion was considerably reduced by CVLE, according to the gravimetric analysis's findings. In particular, at 1000 ppm and 298 K, the inhibitory efficiency (IE%) of CVLE was determined to be 91.83 ± 0.04%. It was discovered that the inhibition efficacy of CVLE rose with concentration but fell with temperature.

• The results of the potentiodynamic polarization demonstrate that the CVLE inhibitor modulates both the cathodic and anodic responses. This implies that the inhibitor behaves in a mixed manner.

• According to the EIS investigation, CVLE increases the positive aspects of charge transfer resistance (R_{ct}) and decreases its values when it is present in the destructive medium. This impression demonstrates how CVLE gains strength through adsorption at the metal–electrolyte contacts.

• The R^2 value, which is near 1, was determined to be 0.99807 during the adsorption investigations. The plot of C_{inh} *vs.* C_{inh}/θ yielded a straight curve, indicating that the inhibitor's adsorption onto the mild steel surface in a 1 N HCl solution followed the Langmuir adsorption isotherm.

• Studies using scanning electron microscopy confirmed the noticeable corrosion by demonstrating the development of a protective layer of CVLE on the surface of mild steel. The DFT study revealed that the flat adsorption structure of the adsorbed molecule made it more stable. Moreover, improved surface coverage was the outcome of the metallic surface having more active zones.

Ethical approval

My manuscript has never been submitted to more than one journal for concurrent review elsewhere. The results of this study have not been made public. The results are given honestly, openly, and without any kind of falsification or inappropriate data modification. The authors have carefully collected, selected, and processed data in accordance with field-specific norms. Plagiarism has been scrupulously avoided; there is not a single instance of presenting someone else's data, text, or theories as our own theories as though they were original to us; plagiarism has been avoided at all costs.

Consent for publication

The authors consent to publication, and this work has not been submitted or published in any other journals.

Consent to participate

Every author concurs with the submission's substance and pledges to support the ongoing research.

Data availability

Data will be provided on request.

Author contributions

Aashu Singh Solanki has done the conceptualization and methodology and written the original draft. Abhinay Thakur has done the computational analysis. Shobhana Sharma has done the review and editing. Ankit Sharma has done the formal analysis. Sushil Kumar Sharma has done the validation and supervision.

Conflicts of interest

The authors affirm that none of the research described in this publication is influenced by any known financial interests or personal connections.

Acknowledgements

The authors are highly grateful to the Head of the Department of Pure and Applied Chemistry, University of Kota, Kota, for providing facilities for the department. The authors also thank MRC and MNIT Jaipur for providing spectroscopic facilities.

References

1 H. Aljibori, A. Al-Amiery and W. N. Isahak, Advancements in corrosion prevention techniques, *J. Bio-Tribo-Corros.*, 2024, **10**, 78, DOI: 10.1007/s40735-024-00882-w.

2 Z. I. Jasim, K. H. Rashid and A. A. Khadom, Corrosion and Corrosion Control of the Steel in Acidizing Oil Wells Processes: An Overview of Organic Inhibitors, *Russ. J. Appl. Chem.*, 2024, **10**, 1–9, DOI: 10.1134/S1070427224010063.

3 H. Zhang and H. Q. Lan, A review of internal corrosion mechanism and experimental study for pipelines based on multiphase flow, *Corros. Rev.*, 2017, **35**, 425–444, DOI: 10.1515/corrrev-2017-0064.

4 S. Sharma, A. Jain and S. Saxena, Incorporation of Titanium (IV) into Sterically Hindered Schiff Bases of Heterocyclic β-

Diketones Involving Ketooximes and Glycol as Coligands: Preparation and Structural Considerations, *Phosphorus, Sulfur Silicon Relat. Elem.*, 2009, **184**, 1676–1688, DOI: 10.1080/10426500802176598.

5 S. Sharma, A. Jain and S. Saxena, Some Zirconium (IV) Complexes of Sterically Constrained Sulfur-Containing Schiff Bases of Heterocyclic β-Diketones: Synthetic Strategy and Structural Investigation Based Upon Spectroscopic Studies, *Phosphorus, Sulfur Silicon Relat. Elem.*, 2009, **184**, 1689–1701, DOI: 10.1080/10426500802176614.

6 S. Sharma, A. Jain and S. Saxena, Synthesis, characterization and antimicrobial activity of zirconium (IV) complexes, *J. Korean Chem. Soc.*, 2012, **56**, 440–447, DOI: 10.5012/jkcs.2012.56.4.440.

7 S. Sharma, Structure-activity relationship of some pentacoordinated Tributyltin (IV) complexes derived from sterically hindered Schiff bases of heterocyclic β-diketones, *J. Indian Chem. Soc.*, 2022, **99**, 100464, DOI: 10.1016/j.jics.2022.100464.

8 S. Sharma, Y. K. Paridwal, S. Sharma, A. Sharma and S. K. Sharma, Synthesis, characterization, and computational study of N-protected amino acid inhibitors as well as assessment of corrosion resistance properties on mild steel in. 5 M H_2SO_4 solution, *Asia-Pac. J. Chem. Eng.*, 2023, **18**, e2959, DOI: 10.1002/apj.2959.

9 A. Rathore, S. Sharma, A. Sharma and S. K. Sharma, Evaluation of structure-reactivity correlation of efficient corrosion inhibitor ionic liquids for mild steel in acidic medium, *J. Dispersion Sci. Technol.*, 2024, **45**, 1107–1119, DOI: 10.1080/01932691.2023.2197996.

10 S. Gurjar, S. Ratnani, S. K. Sharma and S. Sharma, Adsorption of Ionic Liquids on The Metal Surface: Co-ordination Chemistry Of Ionic Liquids, *Ionic Liquids: Eco-Friendly Substitutes for Surface and Interface Applications*, ed. C. Verma, Bentham Science Publishers, Singapore, 2023, pp. 77–92, DOI: 10.2174/9789815136234123010 1.

11 N. Benachour, A. Delimi, H. Allal, A. Boublia, A. Sedik, H. Ferkous, A. Djedouani, S. Brioua, C. Boulechfar, H. Benzouid and A. Houssou, 3, 4-Dimethoxy phenyl thiosemicarbazone as an effective corrosion inhibitor of copper under acidic solution: comprehensive experimental, characterization and theoretical investigations, *RSC Adv.*, 2024, **14**(18), 12533–12555, DOI: 10.1039/D3RA08629A.

12 N. Mouats, S. Djellali, H. Ferkous, A. Sedik, A. Delimi, A. Boublia, K. O. Rachedi, M. Berredjem, A. Çukurovali, M. Alam and B. Ernsti, Comprehensive investigation of the adsorption, corrosion inhibitory properties, and quantum calculations for 2-(2, 4, 5-trimethoxybenzylidene) hydrazine carbothioamide in mitigating corrosion of XC38 carbon steel under HCl environment, *ACS Omega*, 2024, **9**(26), 27945–27962, DOI: 10.1021/acsomega.3c10240.

13 A. Madaci, H. Ferkous, A. Sedik, A. Delimi, C. Boulechfar, A. Belakhdar, M. Berredjem, M. A. Chaouch, M. Alam, H. Majdoub and N. Jaffrezic-Renault, Experimental and theoretical study of polysaccharides extracted from prickly pear nopales Pulp (PPUN) of Opuntia ficus-indica as corrosion inhibitors, *J. Mol. Liq.*, 2023, **384**, 122272, DOI: 10.1016/j.molliq.2023.122272.

14 S. Brioua, A. Delimi, H. Ferkous, S. Boukerche, H. Allal, A. Boublia, A. Djedouani, M. Berredjem, A. Kahlouche, K. O. Rachedi and A. Abdennouri, Enhancing corrosion resistance of XC38 steel using sulfur and nitrogen-containing phenyl thiosemicarbazone: A comprehensive experimental and computational analysis, *J. Taiwan Inst. Chem. Eng.*, 2024, **165**, 105718, DOI: 10.1016/j.jtice.2024.105718.

15 T. Himeur, K. Rouibah, H. Ferkous, A. Boublia, K. O. Rachedi, K. Harrouche, C. Boulechfar, A. Abdennouri and Y. Benguerba, Unlocking the power of Inula Viscosa essential oil: A green solution for corrosion inhibition in XC48 steel within acidic environments, *Process Saf. Environ. Prot.*, 2024, **187**, 1422–1445, DOI: 10.1016/j.psep.2024.05.061.

16 I. Lakikza, Y. Benguerba, A. Boublia, S. I. Aouni, H. Lahbib, H. Ferkous, H. Ghodbane, Y. Benamor, A. S. Bentalib and B. Ernst, Comprehensive evaluation of Alysicarpus compactum extract as a natural corrosion inhibitor for St37 carbon steel in acidic media, *J. Ind. Eng. Chem.*, 2025, **147**, 161–178, DOI: 10.1016/j.jiec.2024.12.010.

17 S. Sharma and A. Singh, Synthesis of Graphene-Based Nanomaterials for Medicinal Applications: A Mini-Review, *Curr. Org. Chem.*, 2022, **26**, 1112–1118, DOI: 10.2174/1385272826666220621141128.

18 P. Sharma, S. Sharma, S. K. Sharma, A. Jain and K. Shrivastava, Review on Recent advancement of adsorption potential of sugarcane bagasse biochar in wastewater treatment, *Chem. Eng. Res. Des.*, 2024, **206**, 428–439, DOI: 10.1016/j.cherd.2024.04.055.

19 P. Sharma, S. Sharma, S. K. Sharma, S. Yifei, F. Guo, T. Ichikawa, A. Jain and K. Shrivastava, Evaluation of optimized conditions for the adsorption of malachite green by SnO_2-modified sugarcane bagasse biochar nanocomposites, *RSC Adv.*, 2024, **14**, 29201–29214, DOI: 10.1039/D4RA05442C.

20 S. Sharma, A. S. Solanki and S. K. Sharma, Anticorrosive action of eco-friendly plant extracts on mild steel in different concentrations of hydrochloric acid, *Corros. Rev.*, 2024, **42**, 185–201, DOI: 10.1515/corrrev-2023-0053.

21 S. Sharma, A. S. Solanki, A. Thakur, A. Sharma, A. Kumar and S. K. Sharma, Phytochemicals as eco-friendly corrosion inhibitors for mild steel in sulfuric acid solutions: a review, *Corros. Rev.*, 2024, **42**, 727–742, DOI: 10.1515/corrrev-2024-0018.

22 S. Sharma, S. Gurjar, S. Ratnani and S. K. Sharma, Synthesis, Characterization, and Applications of Surface Modified Carbon Nanotubes, in *Surface Modified Carbon Nanotubes Volume 1: Fundamentals, Synthesis and Recent Trends*, ed. J. Aslam, C. M. Hussain and R. Aslam, American Chemical Society, Washington, DC, 2022, pp. 49–65, DOI: 10.1021/bk-2022-1424.ch003.

23 S. Sharma, A. Sharma and S. K. Sharma, Ecotoxicological effects and socio-economical aspects of nanoadsorbent materials, in *Adsorption through Advanced Nanoscale*

Materials, ed. C. Verma, J. Aslam and E. Khan, Elsevier, Amsterdam, Netherlands, 2023, pp. 507–531, DOI: 10.1016/B978-0-443-18456-7.00023-7.

24 S. Sharma, A. Sharma, S. K. Sharma and A. Thakur, Encapsulation of Metal/Metal Oxide Nanoparticles as Corrosion Inhibitors, in *Encapsulated Corrosion Inhibitors for Eco-Benign Smart Coatings*, ed. A. Kumar and A. Thakur, CRC Press, Boca Raton, 2024, pp. 46–62. doi: DOI: 10.1201/9781032677255.

25 A. Thakur, S. Kaya, A. S. Abousalem, S. Sharma, R. Ganjoo, H. Assad and A. Kumar, Computational and experimental studies on the corrosion inhibition performance of an aerial extract of Cnicus Benedictus weed on the acidic corrosion of mild steel, *Process Saf. Environ. Prot.*, 2022, **161**, 801–818, DOI: 10.1016/j.psep.2022.03.082.

26 U. Mamudu, M. S. Alnarabiji and R. C. Lim, Adsorption isotherm and molecular modeling of phytoconstituents from Dillenia suffruticosa leaves for corrosion inhibition of mild steel in 1.0 M hydrochloric acid solution, *Res. Surf. Interfaces*, 2023, **13**, 100145, DOI: 10.1016/j.rsurfi.2023.100145.

27 A. Thakur, O. Dagdag, A. Berisha, E. E. Ebenso, A. Kumar, S. Sharma, R. Ganjoo and H. Assad, Mechanistic insights into the corrosion inhibition of mild steel by eco-benign Asphodelus tenuifolius aerial extract in acidic environment: electrochemical and computational analysis, *Surf. Coat. Technol.*, 2024, **480**, 130568, DOI: 10.1016/j.surfcoat.2024.130568.

28 B. Tan, Z. Gong, W. He, J. Xiong, L. Guo and R. Marzouki, Insight into the anti-corrosion mechanism of crop waste Arachis hypogaea L. leaf extract for copper in sulfuric acid medium, *Sustainable Chem. Pharm.*, 2024, **38**, 101449, DOI: 10.1016/j.scp.2024.101449.

29 E. M. Njoya, P. M. Fewou and T. H. Niedermeyer, Codiaeum variegatum (L.) Rumph. ex A. Juss.(Euphorbiaceae): An overview of its botanical diversity, traditional uses, phytochemistry, pharmacological effects and perspectives towards developing its plant-based products, *J. Ethnopharmacol.*, 2021, **277**, 114244, DOI: 10.1016/j.jep.2021.114244.

30 A. S. Fouda, M. A. Azeem, S. A. Mohamed, A. El-Hossiany and E. El-Desouky, Corrosion inhibition and adsorption behavior of nerium oleander extract on carbon steel in hydrochloric acid solution, *Int. J. Electrochem. Sci.*, 2019, **14**(4), 3932–3948.

31 S. I. Ezugha, C. C. Aralu and V. C. Eze, Inhibition potentials of Solanum macrocarpon leave extract as a green corrosion inhibitor of mild steel in an acidic solution, *J. Bio- Tribo-Corros.*, 2024, **10**(4), 81.

32 K. P. Kumar, M. Pillai and G. R. Thusnavis, Green corrosion inhibitor from seed extract of Areca catechu for mild steel in hydrochloric acid medium, *J. Mater. Sci.*, 2011, **46**, 5208, DOI: 10.1007/s10853-011-5457-0.

33 S. Gurjar, S. Ratnani, P. Kandwal, K. K. Tiwari, A. Sharma and S. K. Sharma, Experimental and theoretical studies of 1-Benzyl pyridazinium bromide as green inhibitor for mild steel corrosion, *e-Prime-Adv.*, 2022, **2**, 100054, DOI: 10.1016/j.prime.2022.100054.

34 S. Ratnani, S. K. Sharma, C. Verma, S. A. Chaudhry and S. Gurjar, Evaluation of inhibition performance of methylimidazolium ionic liquids on surface of mild steel in sulfuric acid, *Surf. Coat. Technol.*, 2024, **485**, 130875, DOI: 10.1016/j.surfcoat.2024.130875.

35 S. Sharma and I. Mohammad, The computational study, thermodynamic parameters, and partial inhibition of spermatogenesis exhibited by toxicophores scaffolds of an organic–inorganic hybrid complex of tributyltin (IV), *Appl. Organomet. Chem.*, 2022, **36**, e6776, DOI: 10.1002/aoc.6776.

36 S. Sharma, R. Kumar, P. Kumar, A. Jain and S. Saxena, New insights into the predicament of DFT assisted optimized energy, stability and distortions of optimized topologies of some novel complexes of Zirconium (IV) and enhancement of antimicrobial potential, *Appl. Organomet. Chem.*, 2019, **33**, e5080, DOI: 10.1002/aoc.5080.

37 C. Verma, L. O. Olasunkanmi, E. Ebenso, M. A. Quraishi and I. B. Obot, Adsorption behavior of glucosamine-based, pyrimidine-fused heterocycles as green corrosion inhibitors for mild steel: experimental and theoretical studies, *J. Phys. Chem. C*, 2016, **120**, 11598–11611, DOI: 10.1021/acs.jpcc.6b04429.

38 P. Muthukrishnan, K. Saravana Kumar, B. Jeyaprabha and P. Prakash, Anticorrosive activity of Kigelia pinnata leaves extract on mild steel in acidic media, *Metall. Mater. Trans. A*, 2014, **45**, 4510–4524, DOI: 10.1007/s11661-014-2366-2.

39 I. H. Ali and M. H. Suleiman, Effect of acid extract of leaves of Juniperus procera on corrosion inhibition of carbon steel in HCl solutions, *Int. J. Electrochem. Sci.*, 2018, **13**, 3910–3922, DOI: 10.20964/2018.04.01.

40 S. Gurjar, S. K. Sharma, A. Sharma and S. Ratnani, Performance of imidazolium based ionic liquids as corrosion inhibitors in acidic medium: A review, *Appl. Surf. Sci. Adv.*, 2021, **6**, 100170, DOI: 10.1016/j.apsadv.2021.100170.

41 L. Y. Helen, A. A. Rahim, B. Saad, M. I. Saleh and P. B. Raja, Aquilaria crassna leaves extracts-a green corrosion inhibitor for mild steel in 1 M HCl medium, *Int. J. Electrochem. Sci.*, 2014, **9**, 830–846, DOI: 10.1016/S1452-3981(23)07760-X.

42 S. Gurjar, S. K. Sharma, A. Sharma A and S. Ratnani, Pyridazinium based ionic liquids as green corrosion inhibitors: An overview, *Electrochem. Sci. Adv.*, 2022, **2**, e2100110, DOI: 10.1002/elsa.202100110.

43 M. H. Hussin and M. J. Kassim, The corrosion inhibition and adsorption behavior of Uncaria gambir extract on mild steel in 1 M HCl, *Mater. Chem. Phys.*, 2011, **125**, 461–468, DOI: 10.1016/j.matchemphys.2010.10.032.

44 S. Saxena, D. Prasad and R. Haldhar, Investigation of corrosion inhibition effect and adsorption activities of Cuscuta reflexa extract for mild steel in 0.5 M H_2SO_4, *Bioelechem*, 2018, **124**, 156–164, DOI: 10.1016/j.bioelechem.2018.07.006.

45 U. Mamudu, J. H. Santos, S. A. Umoren, M. S. Alnarabiji and R. C. Lim, Investigations of corrosion inhibition of ethanolic extract of Dillenia suffruticosa leaves as a green corrosion

inhibitor of mild steel in hydrochloric acid medium, *Corros. Commun.*, 2024, **15**, 52–62, DOI: 10.1016/j.corcom.2023.10.005.

46 N. S. Patel, S. Jauhariand, G. N. Mehta, S. S. Al-Deyab, I. Warad and B. J. Hammouti, Mild steel corrosion inhibition by various plant extracts in 0.5 M sulphuric acid, *Int. J. Electrochem. Sci.*, 2013, **8**, 2635–2655, DOI: 10.1016/S1452-3981(23)14337-9.

47 A. Fattah-alhosseini and B. Hamrahi, Effect of Thyme Leaves Hydroalcoholic Extract on Corrosion Behavior of API 5L Carbon Steel in 0.5 M H2SO4, *Anal. Bioanal. Chem.*, 2016, **8**, 535–546.

48 S. A. Korniy, S. A. Halaichak, M. R. Chuchman, V. A. Vynar and B. M. Datsko, Effect of anodic treatment on the electrocatalytic activity of electrodeposited Ni-Mo coatings as cathode materials for hydrogen evolution reaction, *Colloids Surf., A*, 2025, **705**, 135677, DOI: 10.1016/j.colsurfa.2024.135677.

49 Z. Bai, Y. Li, L. Xing, P. Gao, Z. Yu, S. Ding, D. Macdonald and S. Wang, In Situ Monitoring Techniques and Analysis Theory for Electrochemical Corrosion in Subcritical and Supercritical Aqueous Systems, *J. Electrochem. Soc.*, 2025, **172**, 021504, DOI: 10.1149/1945-7111/adb33a.

50 M. Huang, R. Wang, J. Xiong, C. Liu, J. Wang and Q. Wang, Inhibition effect and adsorption behavior of Michelia alba leaf extract as corrosion inhibitors for Cu in 0.5 M H2SO4, *J. Dispersion Sci. Technol.*, 2025, 1–8, DOI: 10.1080/01932691.2025.2461110.

51 S. D. Kotabagi, R. L. Minagalavar, S. K. Rajappa, M. R. Rathod and A. M. Sajjan, Evaluation of surface interaction of plant root extract components on mild steel surface in HCl medium: electrochemical, and surface characterization approaches, *Res. Surf. Interfaces*, 2024, **16**, 100275, DOI: 10.1016/j.rsurfi.2024.100275.

52 M. Srivastava, P. Tiwari, S. K. Srivastava, A. Kumar, G. Ji and R. Prakash, Low cost aqueous extract of Pisum sativum peels for inhibition of mild steel corrosion, *J. Mol. Liq.*, 2018, **254**, 357–368, DOI: 10.1016/j.molliq.2018.01.137.

53 M. Mobin, S. Zamindar and P. Banerjee, Mechanistic insight into adsorption and anti-corrosion capability of a novel surfactant-derived ionic liquid for mild steel in HCl medium, *J. Mol. Liq.*, 2023, **385**, 122403, DOI: 10.1016/j.molliq.2023.122403.

54 J. K. Emmanuel, Corrosion protection of mild steel in corrosive media, a shift from synthetic to natural corrosion inhibitors: a review, *Bull. Natl. Res. Cent.*, 2024, **48**, 26, DOI: 10.1186/s42269-024-01181-7.

55 V. Vorobyova, M. Skiba and Z. Julia, A New Combination Inhibitor Based on Tomato Pomace Extract and Organosilane for Enhanced Anticorrosion Performance of Steel, *Chem. Afr.*, 2022, **5**, 997–1014, DOI: 10.1007/s42250-022-00388-3.

56 B. Ran, Y. Qiang, X. Liu, L. Guo, A. G. Ritacca, I. Ritacco and X. Li, Excellent performance of amoxicillin and potassium iodide as hybrid corrosion inhibitor for mild steel in HCl environment: adsorption characteristics and mechanism insight, *J. Mater. Res. Technol.*, 2024, **29**, 5402–5411.

57 M. Lebrini, F. Suedile, P. Salvin, C. Roos, A. Zarrouk, C. Jama and F. &Bentiss, Bagassaguianensis ethanol extract used as sustainable eco-friendly inhibitor for zinc corrosion in 3% NaCl: Electrochemical and XPS studies, *Surf. Interfaces*, 2020, **20**, 100588.

58 N. H. Hashim, A. H. Ali, A. Khatib and J. Latip, Discrimination of Clinacanthus nutans extracts and correlation with antiplasmodial activity using ATR-FTIR fingerprinting, *Vib. Spectrosc.*, 2019, **104**, 102966, DOI: 10.1016/j.vibspec.2019.102966.

59 C. Radulescu C, R. L. Olteanu, C. Stihi, M. Florescu, D. Lazurca, I. D. Dulama, R. M. Stirbescu and S. Teodorescu, Chemometric assessment of spectroscopic techniques and antioxidant activity for Hippophae rhamnoides L. extracts obtained by different isolation methods, *Anal. Lett.*, 2019, **52**, 2393–2415, DOI: 10.1080/00032719.2019.1590379.

60 C. Rong, B. Wang, D. Zhao and S. Liu, Information-theoretic approach in density functional theory and its recent applications to chemical problems, *Wiley Interdiscip. Rev.: Comput. Mol. Sci.*, 2020, **10**, e1461, DOI: 10.1002/wcms.1461.

61 P. Zhang, Y. Yang, X. Duan, Y. Liu and S. Wang, Density functional theory calculations for insight into the heterocatalyst reactivity and mechanism in persulfate-based advanced oxidation reactions, *ACS Catal.*, 2021, **11**, 11129–11159, DOI: 10.1021/acscatal.1c03099.

62 Y. Mu, T. Wang, J. Zhang, C. Meng, Y. Zhang and Z. Kou, Single-atom catalysts: advances and challenges in metal-support interactions for enhanced electrocatalysis, *Electrochem. Energy Rev.*, 2022, **14**, 1–42, DOI: 10.1007/s41918-021-00124-4.

63 A. El Ouaddari, R. Kellal, Z. A. El Caid, R. Albarakati, N. Wazzan, O. S. Al-Qurashi, Z. Safi, S. I. Moussa, A. El Amrani, M. Zertoubi and D. B. Left, Insight into anti-corrosion behavior of Cladanthus mixtus (L.) flower extracts as a biodegradable inhibitor for carbon steel in acid medium: experimental and theoretical studies, *Mater. Chem. Phys.*, 2024, **326**, 129827, DOI: 10.1016/j.matchemphys.2024.129827.

64 R. J. Maurer, V. G. Ruiz, J. Camarillo-Cisneros, W. Liu, N. Ferri, K. Reuter and A. Tkatchenko, Adsorption structures and energetics of molecules on metal surfaces: Bridging experiment and theory, *Prog. Surf. Sci.*, 2016, **91**, 72–100, DOI: 10.1016/j.progsurf.2016.05.001.

65 S. G. Croll, Surface roughness profile and its effect on coating adhesion and corrosion protection: A review, *Prog. Org. Coat.*, 2020, **148**, 105847, DOI: 10.1016/j.porgcoat.2020.105847.

66 S. A. Umoren and M. M. Molomon, Synergistic corrosion inhibition effect of metal cations and mixtures of organic compounds: a review, *J. Environ. Chem. Eng.*, 2017, **5**, 246–273, DOI: 10.1016/j.jece.2016.12.001.

67 S. J. Price and R. B. Figueira, Corrosion protection systems and fatigue corrosion in offshore wind structures: current status and future perspectives, *Coat*, 2017, **7**, 25, DOI: 10.3390/coatings7020025.

68 B. A. Rani and B. B. Basu, Green inhibitors for corrosion protection of metals and alloys: an overview, *Int. J. Corros.*, 2012, **2012**, 380217, DOI: **10.1155/2012/380217**.

69 L. Anggraini, Y. Emriadi, S. Zulaiha and H. Pardi, Stainless 37 Steel Corrosion Inhibition in a Hydrochloric Acid Solution with Senggani (Melastoma Candidum D. Don) Leaf Extract, *Port. Electrochim. Acta*, 2023, **41**(3), 199–210, DOI: **10.4152/pea.2023410302**.

70 H. Gerengi and H. I. Sahin, Schinopsis lorentzii extract as a green corrosion inhibitor for low carbon steel in 1 M HCl solution, *Ind. Eng. Chem. Res.*, 2012, **51**(2), 780–787, DOI: **10.1021/ie201776q**.

71 A. Ishak, F. V. Adams, J. O. Madu, I. V. Joseph and P. A. Olubambi, Corrosion inhibition of mild steel in 1M hydrochloric acid using Haematostaphis barteri leaves extract, *Procedia Manuf.*, 2019, **35**, 1279–1285, DOI: **10.1016/j.promfg.2019.06.088**.

72 A. Ehsani, M. G. Mahjani, M. Hosseini, R. Safari, R. Moshrefi and H. M. Shiri, Evaluation of Thymus vulgaris plant extract as an eco-friendly corrosion inhibitor for stainless steel 304 in acidic solution by means of electrochemical impedance spectroscopy, electrochemical noise analysis and density functional theory, *J. Colloid Interface Sci.*, 2017, **490**, 444–451, DOI: **10.1016/j.jcis.2016.11.048**.

73 M. A. Asaad, M. Ismail, N. H. Khalid, G. F. Huseien and P. B. Raja, Elaeis guineensis leaves extracts as eco-friendly corrosion inhibitor for mild steel in hydrochloric acid, *J. Teknol.*, 2018, **80**(6), 53–59, DOI: **10.11113/jt.v80.11191**.

74 H. Lahbib, S. Ben Hassen, H. Gerengi, M. Rizvi and Y. Ben Amor, Corrosion inhibition performance of dwarf palm and Cynara cardunculus leaves extract for St37 steel in 15% H2SO4: a comparative study, *J. Adhes. Sci. Technol.*, 2021, **35**(7), 691–722, DOI: **10.1080/01694243.2020.1819701**.

75 Z. Jebali, H. Ferkous, M. Zerroug, A. Boublia, A. Delimi, A. Bouzid, H. Majdoub, B. Ernst, N. Elboughdiri and Y. Benguerba, Unveiling the potent corrosion-inhibiting power of Ammophila arenaria aqueous extract for mild steel in acidic environments: An integrated experimental and computational study, *J. Environ. Chem. Eng.*, 2024, **12**(2), 112374, DOI: **10.1016/j.jece.2024.112374**.